Master Thesis in Geographical Information Science nr 131

The hydrodynamic impacts of Estuarine Oyster reefs, and the application of drone technology to this study

Oskar Evert Johansson

2021

Department of

Physical Geography and Ecosystem Science

Centre for Geographical Information Systems

Lund University, Sölvegatan 12, S-223 62 Lund, Sweden

The hydrodynamic impacts of Estuarine Oyster Reefs, and the application of drone technology to this study

---

Oskar E Johansson (2021)

Master degree thesis, 30 credits, Master in Geographical Information Science

Department of Physical Geography and Ecosystem Science, Lund University

Declaration

This thesis is composed of my original work, and contains no material previously published or written by another person except where due reference has been made in the text. I have clearly stated the contribution by others to jointly-authored works that I have included in my thesis. The thesis follows the word count prescribed by the guidelines provided (22,416 words)

Oskar E Johansson

Acknowledgments

First and foremost, I would like to thank A/Prof Ana Vila Concejo for taking me on as a research student. Your ability to keep me from going down “rabbit holes” and directing me back on path was always needed. Your patience and calm nature was exactly what I needed during stressful times and to get this project over the line. To my partner Cornelia Ersson, thank you for putting up with my tired and absent mindedness a lot of this year. You helped me through the whole endeavour and I’m so thankful for your patience. To Abdulghani Hasan, thank you for taking me on as Master research student, it has been a hectic year and hopefully I have not been too much of a hassle. To Tommy Fellowes, although COVID-19 cut our office chats down drastically, you were always available for me to talk things through, to guide me out of any technical issues, or keep me away from the “shiny things”. Finally, to my father Klas Johansson, thank you for the edits and help structuring my writing. I could only hope to one day be half as good a writer as you, but you have certainly inched me closer throughout this process.

Abstract

The impacts of climate change are being seen within the estuarine environment through erosion and shoreline retreat, associated with sea-level rise and changes in storm activity. Restoration oyster reefs have been identified as a working-with-nature strategy to protect and restore these shoreline environments, stabilising sediment, and reducing erosion. Despite restoration projects already being initiated worldwide, their local hydrodynamic impacts are still poorly understood. This is in part due to the dynamic environment that reefs exist in, creating difficulties for surveying and monitoring. The use of digital elevation models (DEMs) is crucial for observing and analysing the hydrodynamics and morphological responses to these large three-dimensional living structures, and the dynamic marine environment has proven problematic for past surveying techniques. Advances in drone technology has the potential to overcome the difficulties of modelling in dynamic marine environments, creating higher resolution and more accurate models. The use of such technologies, paired with hydrodynamic observations, may enable a better understanding of how oyster reefs are influencing the environments in which they exist. It is therefore the aims of this thesis to (1) study the influence of estuarine oyster reefs on the local hydrodynamics and sediment morphology, and (2) incorporate and evaluate the application of drone technology to this study. To achieve these goals, an oyster reef located in the microtidal estuary of Port Hacking, Australia, was selected to collect wave, current, sediment, and topographic data of the reef and surrounding sediment substrate. The results from this research identified the presence of hydrodynamic protection in the leeward direction from both tidal currents and local wind waves, developing a significant sediment accretion area within this protection zone, extending many times the size of the reef. Wave attenuation characteristics by the reef were found to be similar to man-made engineering structures, such as sea walls/breakwaters, where waves were able to pass over the reef freely when the reef

is completely submerged, but blocked from passing when the reef is exposed. Evidence of higher energy wave dissipation was also present, likely from artificial sources such as local boat and ferry traffic. These results build on past research that has identified an increased amount of sediment on the leeward side of the reef, by illustrating the spatial patterns and extent of influence oyster reefs have on the local morphology and surrounding sediment substrate. Such findings emphasise the use of oyster reefs as a natural engineering structure, mimicking the functionality of man-made structures while providing additional ecosystem services by creating, developing, and maintaining habitat for other species on an estuary wide scale. However, the significant scale of hydrodynamic and morphological influence from reefs highlights their possibility to interfere with the natural sediment transport within these dynamic estuarine systems, a process which is relied upon by various ecosystems. Therefore, a broader scale perspective must be taken to understand restorative and hydrodynamic impacts on the wider estuarine system. The high resolution and low resources required for drone data collection presents as a highly promising and feasible avenue to continue these studies, enabling higher frequency surveys to monitor changes over time. Continuing research into oyster reef restoration is key to improving our understanding of the role oyster reefs can play in restoring the health of already degraded estuarine systems, with the potential to benefit the vast communities that both rely on and enjoy their natural resources.

Table of Contents

List of abbreviations, notations, and terminology

AHD	Australian Height Datum
BOM	Bureau Of Meteorology
DEM	Digital Elevation Model
GCP	Ground Control Point
GDA	Geocentric Datum of Australia
GPS	Global Positioning System
H_s	Significant Wave Height
ka	Thousand years ago
LiDAR	Light Detection and Ranging
MHL	Manly Hydraulics Laboratory
MSL	Mean Sea Level
NSW	New South Wales
PAEK	Polynomial Approximation with Exponential Kernel
RMSE	Root Mean Square Error
RTK-GNSS	Real-Time Kinematic Global Navigation Satellite Systems
s	Seconds
SD	Standard Deviation
SFM	Structure From Motion
SIMS	Sydney Institute of Marine Science
TIN	Triangular Irregular Networks
TLS	Terrestrial Laser Scanning

TN	True North
UAS	Unmanned Aerial System
UAV	Uncrewed Aerial Vehicle
Ebb	The tidal phase when water is moving out to sea
Hydrodynamics	The study of fluid motion and the associated forces acting on immersed solid bodies
Morphology	The structure and shape of landforms in relation to topographic features

List of Tables

List of Figures

1 Introduction

1.1 Scientific Rationale

The Australian coastline consists of more than 738 estuaries (Kench, 1999), the transition zone where saline oceanic waters mix with freshwater discharge from rivers, creating unique aquatic environments where salinity varies temporally and geographically (Potter et al., 2010). They house some of the most biologically rich and productive ecosystems, responsible for sustaining the biological resources of our coastline (Viles and Spencer, 2014). Named as one of Australia's most valuable natural resources (Smith et al., 2001), estuaries provide economic benefits through their use for transportation, harbour ports, urban and industrial shoreline development, aquaculture and fisheries operations, as well as tourist attractions (Harris et al., 2016a). Estuaries also provide non-monetary values through social and cultural importance, such as recreational activities, as well as historic, spiritual, or religious significance (Barbier et al., 2011). The health of these systems, defined as the maintenance of estuarine ecosystems structure and function (Van Niekerk et al., 2013), is closely linked to their value (Barbier et al., 2011, Pendleton, 2009). As the health of the system changes, so too does the production value for fisheries and aquaculture, as well as the attraction value for tourists and recreational users.

One of the most important contributors to estuarine health is oyster reefs (Alleway and Connell, 2015). These 3-dimensional aggregate structures of living and dead shell accumulate form a hard substrate in a mostly soft-sediment environment (Grabowski and Peterson, 2007), feeding on suspended sediment delivered by local currents and waves. Oyster reefs play a critical role as ecosystem engineers (Jones et al., 1994) by creating, developing, and maintaining habitat for other species on a system-wide scale (McLeod et al., 2019). They also improve water quality by acting as an ecological filter,

removing nutrients, sediments, and phytoplankton from the water column (Grabowski and Peterson, 2007, Reidenbach et al., 2013).

Historically the exploitation of estuaries for economic value has led to an immense degree of deterioration in their health (Barbier et al., 2011). Intense industrialisation and urbanisation of shorelines, stemming from historic settlement trends of harbour communities, has placed detrimental pressures on estuaries (Mayer-Pinto et al., 2015). Pollution, declining water qualities, overexploitation of resources, and habitat destruction, are some of the anthropogenic pressures causing an aggressive decline in estuarine health (Lotze et al., 2006). This decline has also been seen for oyster reefs, with Australia experiencing immense reef decline throughout the mid-1800s to early 1900s due to overharvesting for both food and lime production, ecosystem modification, and a declining water quality (Alleway and Connell, 2015, Gillies et al., 2018). This dramatic decline has led to only 4% of oyster reef ecosystems built by Australia's two most common reef building oysters (*Saccostrea glomerate* and *Ostrea angasi*) remaining in their historic locations (Gillies et al., 2018).

Ecosystem restoration has increasingly become a strategy for repairing past destructive anthropogenic practices. This strategy extends to oyster reefs, as they are increasingly recognised for their important role in restoring and maintaining ecosystem health (Gillies et al., 2018). While reef restoration projects have already been initiated in Australia, there is still a lack of understanding of their impacts (Gillies et al., 2018). Consequently, there is a need for research aimed at understanding the biological, physical, ecological, and economic impacts of oysters (Campbell and Hall, 2019). One topic of interest is the interactions of hydrodynamics and oyster reefs, which supports the sediment food delivery mechanisms to oyster reefs. This topic has received considerable attention sparked by a recognition that oyster reefs could play a role in moderating climate change impacts by stabilising shorelines and preventing erosion through reducing current velocities, dampening waves, and trapping sediment (Spalding

et al., 2014). While the potential of oyster reefs is commonly cited, the hydrodynamic influence of oyster reefs is still poorly understood with past research being largely inconclusive (Campbell and Hall, 2019). Furthering such research is a key step in understanding the physical and biological impacts of restoration projects.

With advances in field surveying and monitoring technologies, specifically drones, it is now possible to collect new types of data with higher resolution and spatial accuracy (Langhammer et al., 2017). Combined with software, drones can develop highly accurate 3-dimensional models of objects and surfaces from aerial imagery, using photogrammetric techniques (Gonçalves and Henriques, 2015). For the study of oyster reefs and hydrodynamics, this enables greatly improved mapping of reef structures and surrounding sediment morphology, making it possible to better explain hydrodynamic processes (Hart and Martinez, 2006). Such technologies have not yet been applied to the study of oyster reefs elsewhere, and it is the goal of this study to incorporate the advancement of drone data collection in a hydrodynamic analysis to provide some insights into the implications of restorative oyster reef projects and their influence on local hydrodynamics.

1.2 Aims and Objectives

The purpose of this thesis is to better understand the role of oyster reefs in local hydrodynamics, and to incorporate and evaluate the use of drone technology to further this understanding. The aims and objectives to achieve this are as follows:

Aim 1: Do oyster reefs influence local hydrodynamics?

Objectives: (1) Observe and analyse environmental data to identify the interactions between an oyster reef and local hydrodynamics.

(2) Identify the capacity of an oyster reef to shape the morphology of its surrounding environment.

Aim 2: Does drone data collection and processing benefit the hydrodynamic study of oyster reefs?

Objective: (1) Process drone data through Structure From Motion (SFM) techniques to develop a 3-dimensional model of an oyster reef and surrounding sediment substrate.

(2) Quantitatively and qualitatively evaluate drone data collection methods and results to previous techniques of 3-dimensionally modelling oyster reefs.

1.3 Outline

This thesis achieves the aims listed above by following the scientific method. Firstly, Chapter 2 outlines the background to the problem, Chapter 3 follows with an overview of the study area. Chapter 4 includes a detailed description of the methodologies for data collection and analysis. Chapter 5 outlines the main results, and, Chapter 6 presents a discussion of these results in context with existing knowledge. The final conclusions, addressing the aims of the thesis, are in Chapter 7.

2 Background

This chapter is broken into two sections; Estuarine Environments, and drone Technology are their headings, respectively. The first section explores the history and relationships of oyster reefs to estuaries, and how their health has been shaped by human influence. The second section outlines the history and technological advancements of drones, as well as their growing application and potential to coastal science, and more specifically to oyster reefs.

2.1 Estuarine Environments

This section gives background information on estuarine environments, including how they have formed historically and the ecosystems located therein that have developed. Further detail is given on human – estuary interactions, including their value to and impacts from human exploitation, as well as protection and restoration efforts. The final section explores the hydrodynamic and morphological components of an estuary, and the role of oyster reefs in this environment.

2.1.1 Estuary Formation

Estuaries are coastal bodies of water where saline oceanic waters mix with freshwater discharge from rivers and streams (Potter et al., 2010). The formation of most estuaries occurred during the Holocene sea-level rise around 10,000 to 12,000 years ago which flooded coastal valleys, that were initially eroded by rivers or gouged by glaciers (Wolanski and Elliott, 2015). Once established, estuaries began to fill in with either oceanic sediment from the sea floor carried in by tidal currents or terrestrial sources, such as sand, mud, and gravel transported by rivers, rain, and streams. Rates of infilling vary between estuaries and depend on the sediment sources available; rates of deposition, transportation, and erosion depend on local hydrodynamic conditions. If the influx of sediment continues to be greater than the outflow, the estuary matures quicker

and it can eventually fill in completely, becoming dry land. This can also occur from tectonic activity, for example, earthquakes, which can cause uplifts that expose the sediment substrate and dry out the estuary. These different stages of infilling allow for the classification of estuarine maturity, with younger estuaries classified as immature (Jiang et al., 2013).

2.1.2 Estuarine Ecosystems

Regarded as one of the most productive natural habitats in the world (McLusky and Elliott, 2004), estuarine environments are incredibly dynamic zones, where the habitats of marine and riverine species interact. The influence of both land and sea develops a wide variety of habitats, that exist not in isolation but linked by physical, biological, and chemical factors (Meire et al., 2005). Such habitats include seagrass, oyster reefs, salt marshes, mangroves, rocky shorelines, and mud flats to name a few. Governed particularly by the steep salinity gradient from oceanic to freshwaters, species mostly exist in a decreasing abundance moving away from their natural conditions (Wolanski and Elliott, 2015, McLusky and Elliott, 2004). These dynamic and interactive conditions promote the strong biodiversity of estuaries (Kench, 1999, Viles and Spencer, 2014).

2.1.3 Value of Estuaries

The health of estuaries is of significant importance and it accounts for ecological, economic, social, and cultural values (Harris et al. 2016); they are considered one of Australia's most valuable natural resources (Smith et al. 2001). From an economic perspective, estuaries sustain aquaculture and fisheries, provide attraction value for harbour side development, tourism and recreations, and commercial value for port facilities and transportation. Despite estuaries and near shore vegetation only accounting for 0.7% of global biomes, they account for 23.7% of total global ecosystem services, or $7.9 trillion US dollars annually (Scyphers et al., 2011). The ecological

value of estuaries has a strong link to their economic value, as a healthy ecology will produce higher yield for fishery and aquaculture industries, both within estuaries and the coastal regions, as well as increased attraction for tourism industries (Mayer-Pinto et al., 2015). The recreational use of estuaries is of high social importance through the various activities supported, such as swimming, diving, fishing, surfing and boating. Considering that 60% of the world's population lives along estuaries or coastal zones (Harris et al., 2016b), they are a significant social asset. Estuaries also hold a strong cultural value from natural or human history, and for spiritual or religious importance (Barbier et al., 2011). Maintaining their health extends well beyond their economic value, but to the global communities that enjoy and benefit from their services.

2.1.4 Human Impacts

The history of humans and estuaries dates back thousands of years, with initial settlements guided by the abundance of food (Day Jr et al., 2012). Signs of adverse impacts are evident as early as the middle ages through the commercial exploitation of estuarine fish populations. This occurred in European settlements that originally gained their subsistence livelihoods from estuarine resources before transitioning to commercial exploitations (Hoffmann, 2005). A similar time saw changes in land use practices, with the expansions of agricultural land use and increased woodland clearing, resulting in increased erosion and changes to the hydraulic regime. This had unintended adverse impacts on the water quality, habitat, and biodiversity of estuaries (Hoffmann, 2005).

Throughout human history, estuaries have seen significant impacts as they provide natural transportation hubs, where sea and river traffic meet in a sheltered environment. With rising commerce, estuaries quickly grew into port locations to load and unload transportation vessels (Mayer-Pinto et al., 2015). The growth of trade and technological advancements saw dredging operations to accommodate the increase in boat traffic and

larger vessels (McLusky and Elliott, 2004). Shorelines also became cost-effective locations for large scale industry, giving rise to intense shoreline industrialisation and reclamation of land (Harris et al., 2016b). This had significant impacts on the loss of habitat as muddy tidal flats proved to be ideal development locations (Mayer-Pinto et al., 2015, Birch, 2006). Land use changes further increased erosion and sedimentation rates, combined with continued dredging to maintain navigation channels, which translated to an increase in suspended sediment and turbidity (Lotze et al., 2006). Impacts of this can be seen through the deterioration of sub-aquatic vegetation communities from decreased light penetration and changes in sediment dynamics (Vermaat et al., 1997). Industries occupying reclaimed land also utilised the estuarine environment as a convenient waste repository, such as metal foundries and paint manufacturers, severely polluting estuaries with heavy metal contaminants (Birch, 2006). These practices are still of consequence today, with toxic contamination having adverse effects on people ranging from cancers, weakening immune systems, to even fatal poisoning (Simcock et al., 2016).

Historically, industrialisation of estuaries has had a significant correlation to urbanisation (Gollin et al., 2016). Besides further reclamation for development, urbanisation affects estuaries by deteriorating water quality through increased polluted stormwater runoff, solid waste, organic pollution and sewage inputs (Adams et al., 2019, Harris et al., 2016b, McLusky and Elliott, 2004). An example of these impacts can be seen in the Clyde Estuary, Scotland, where the entire fish population was eliminated by 1845-1850 due to industrial and urban development (McLusky and Elliott, 2004). The extent to which estuaries have shaped the urban and industrial development is highlighted by 22 of the 32 largest cities in the world being located beside an estuary (Harris et al., 2016b). Such vast development trends continue to pose a threat into the future of estuaries, particularly with the ever-growing risks of climate change. An example is the concern for sea-level rise and the subsequent drowning of habitats as man-made structural shorelines prohibit the natural landward migration of

coastal wetlands (Spalding et al., 2014). The monitoring, planning, protection, and restoration of these environments is an ongoing task and continues to pose new challenges.

2.1.5 Protecting and Restoring Estuaries

The recognition of severe degradation and pollution of estuarine environments has led to a transition towards restoration over the last few decades (Day Jr et al., 2012, Mayer-Pinto et al., 2015). Different strategies are employed based on the state of the estuary, and the conditions that persist. For water quality problems, such as pollution and eutrophication, national and local scale policies have been enforced to regulate the discharge from domestic and industrial waste, as well as storm water and other contaminant run-off. Examples of this include the Australian *Protection of the Environment Operations Act 1997* (EPA, 1997) and the *United States Environmental Protection Agency Clean Water Act of 1987 (Kovalic, 1987),* which both regulate point source discharges into estuarine environments. For habitat and species protection, zoning is a common practice employed worldwide to restrict access and activities to threatened or ecologically significant areas (Fang et al., 2018). This is a complex process that balances the conservation objectives with spatially varying resource use (Bruce and Eliot, 2006). Such marine zoning practices have been adopted into a legal framework in Australia, USA, Canada and the European Union (Fang et al., 2018).

Increasingly, the trends of coastal management have moved to a more holistic and integrated approach, in order to address the interests of various stakeholders (Caton and Harvey, 2010, Christie, 2005). Examples of this include the *Estuary Habitat Restoration Council* in the U.S. and the *Marine Estate Management Authority* in New South Wales, Australia. This approach has also seen the establishment of intergovernmental treaties, such as the *RAMSAR Convention on Wetlands* that promotes the conservation of wetlands worldwide (Gardner and Davidson, 2011). Such

intergovernmental initiatives are important for conservation projects as ecosystem boundaries and species migration extends beyond the confines country borders (Gardner and Davidson, 2011).

2.1.6 Hydrodynamics and Morphology

Hydrodynamics is the study of forces acting on or from a fluid. In estuarine environments, these forces include those controlled by tidal currents, oceanic waves, freshwater discharge, wind speed, and topographic parameters of length, depth, and width (Levasseur et al., 2007). The scale of the hydrodynamic analysis is also important, where more localised conditions can be controlled by topographical features or restrictions (Kjerfve, 2018). The hydrodynamic conditions of an estuary control the sediment processes of transportation, deposition, and erosion therein, subsequently affecting morphological changes in the sediment substrate. Parameters that further influence this include the sediment particle properties, including size, shape, density and composition (Jiang et al., 2013), where smaller and lighter sediment require less energy to be transported and deposited. Morphological changes also influence the hydrodynamics, such as how tides and waves are able to attenuate throughout the estuary (Jiang et al., 2013). These co-dependent processes create a very dynamic and complex relationship between morphology and hydrodynamics, but understanding and predicting them is key for planning and sustaining a healthy estuarine environment (Jiang et al., 2013, Levasseur et al., 2007).

2.1.7 Role of Oyster Reefs

One of the major contributors to estuarine health is oyster reefs (Alleway and Connell, 2015). Oysters are bivalve molluscs that live in marine or brackish habitats; some species at high densities can form aggregated 3-dimensional reef structures of living and dead shell accumulations (McLeod et al., 2019, Gillies et al., 2018). They are filter feeding organisms that rely on the tidal flushing of the coastal zone to deliver food of

suspended plankton and particles (O'Neil et al., 2016). Over the last 100 years, a decline of about 85% in oyster reef populations has been seen globally, primarily due to overharvesting for food and lime production, ecosystem modifications and a decline in water quality (Rodriguez et al., 2014, Gillies et al., 2018, Alleway et al., 2015). This is particularly the case in Australia, where as little as 4% of ecosystems built by Australia's two most common reef building oysters (*Saccostrea glomerate* and *Ostrea angasi*) remain in their historic location (Gillies et al., 2018).

Oyster reefs play a critical role as ecosystem engineers (Jones et al., 1994) that create, develop, and maintain habitat for other species on a system wide scale (McLeod et al., 2019). They improve water quality by acting as an ecological filter, removing nutrients, sediments, and phytoplankton from the water column (Grabowski and Peterson, 2007, Reidenbach et al., 2013). An expanding understanding of the role of oyster reefs in estuarine health has led to increased interest and investment into restorative oyster reef projects (Lunt et al., 2017, O'Neil et al., 2016). With the ever present threat of climate change, oyster reefs have also been identified as natural moderators, as they stabilise shorelines and prevent erosion through reducing current velocities, dampening waves, and trapping sediment (Spalding et al., 2014). This sort of approach is appealing to coastal management over conventional engineering structures, as it is low in cost and maintenance, as well as being adaptive to environmental changes (Scyphers et al., 2011).

Despite this widely realised importance of oyster reefs, there remains a lack of understanding on how they affect physical and biological processes (Campbell and Hall, 2019, Gillies et al., 2018). One topic of interest is the interactions of hydrodynamics and oyster reefs, which supports their sediment food delivery mechanisms. These interactions are still poorly understood, as past research has been largely inconclusive (Campbell and Hall, 2019). This thesis aims to improve this understanding by investigating the relationship between oyster reefs and the local hydrodynamics.

2.2 Drone Technology

Drones are uncrewed and reusable motorized aircrafts that are operated either by a human pilot, flown autonomously, or a combination of the two (Nex and Remondino, 2014). There are several alternatively used terms for drones, including UAV (Uncrewed Aerial Vehicle), remotely operated aircraft, and remotely piloted vehicle to name a few. Drones are just one part of the uncrewed aerial system (UAS) which comprises of a drone, ground controller, and a system that facilitates the communication between (Gertler, 2012). While the term UAV or UAS is still commonly associated with unmanned aerial vehicles/systems, the use of more inclusive language has led to the transition from 'unmanned' to 'uncrewed'.

The following section outlines the history and development of drone technology, the photogrammetric techniques that facilitate 3-dimesnional modelling of drone data, the technologies evolution in coastal science, and its potential to be applied to oyster reef research.

2.2.1 Drone History

The history of drones stems from a primarily military background, motivated by the application of performing uncrewed reconnaissance, surveillance, strikes, and mapping of hostile areas (Nex and Remondino, 2014). By modern drone definitions, the technology has been around for about 30 years (Gupta et al., 2015). However, early military developments using uncrewed aircraft can be traced back as early as 1849 where uncrewed balloons carrying explosives and a timed fuse were used by Austrians to attack Venice (Naughton, 2007). Although problematic due to no human control and changing weather conditions, the first development of motorised 'drones' took place throughout the 1920s in Britain, creating a radio-controlled aircraft that was used for gunnery target practice by the Royal Navy (Dalamagkidis et al., 2012). This technology became increasingly popular throughout World War II and was soon after identified for

its reconnaissance potential by the US, where aircraft were fitted with cameras capable of 30 minute flight times (Zaloga, 2011). This began the mapping capabilities of uncrewed aircraft, with design and technological developments allowing for increased flight times, and higher resolution imagery (Zaloga, 2011). Although these advancements were all still for military purposes, research groups began realising the mapping potential of drones in the late 1970s (Colomina and Molina, 2014). Despite this happening several decades ago, the widespread application of drones for data collection is only recent. This can be attributed to the spread of low-cost commercially available drones, as well as digital cameras, and global navigation satellite systems (GNSS), all required to navigate and predict points for georeferencing data (Nex and Remondino, 2014).

2.2.2 Photogrammetry and Structure From Motion (SFM)

Photogrammetry is the science of obtaining quantitative measurements about physical objects or the environment from photographic or electromagnetic images (Linder, 2009). There are different techniques and approaches that depend on data availability, and output requirements. One technique that has gained considerable attention is Structure From Motion (SFM). This photogrammetric technique uses stereographic methods to identify 3-dimensional structures from a series of overlapping (Figure 2.1) (Westoby et al., 2012). Its popularity has emerged from the low-cost and high-resolution outputs possible with consumer grade equipment, in particular drones (Mlambo et al., 2017). One of the further benefits of this technique is the ability to spatially-orient models to an absolute coordinate system by using Ground Control Points (GCPs), identifiable points in the model with known spatial coordinates (Westoby et al., 2012), to create digital elevation models (DEMs). The development of georeferenced SFM models is possible in single software packages, such as Agisoft Metashape Professional or Pix4D.

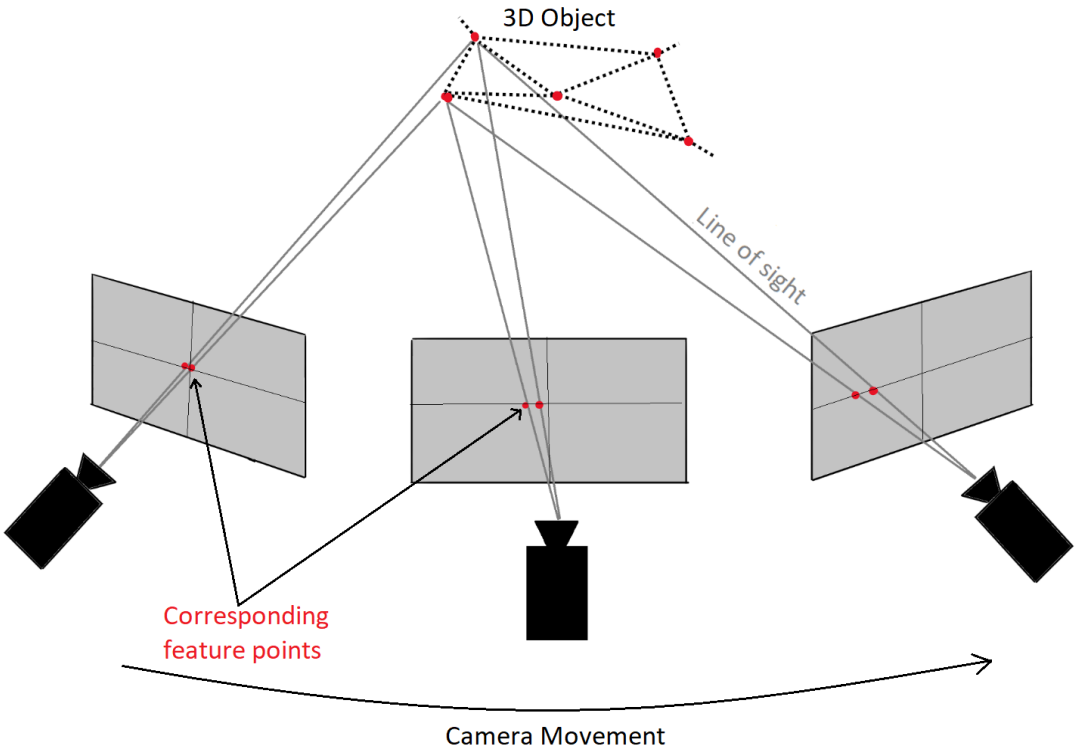

Figure 2.1. Structure From Motion (SFM) principle. Overlapping images of corresponding feature points from different locations/angles allow for points to be located and oriented in 3-dimensional space.

2.2.3 Evolution of Drones in Coastal Science

The increasing availability of digital elevation models (DEMs) with high accuracy and resolution has importance for all sciences interested in 3-dimensional modelling of the environment. This is of particular interest to the coastal sciences, where topographic modelling of sediment surfaces is commonly used to monitor and understand dynamic geomorphological processes over time (Mancini et al., 2013). Past methods to acquire such DEMs have been dominated by airborne LiDAR (Westoby et al., 2012), instruments that emit laser light pulses and record return times to identify distances from source, and process this information to develop a DEM. This technique requires mounting a LiDAR device to a crewed aircraft and flying over the survey area, with potentially multiple passes required to cover the area. Although this technique is high in accuracy and resolution, its application to small scale and high frequency coastal surveys is often impractical (Seymour et al., 2018) due to the prohibitively high costs involved (Westoby et al., 2012, Klemas, 2015). Where LiDAR surveys have been

completed of the coastal zone, sampling frequency has typically been every few years (Drummond et al., 2015). Popular alternatives have included the use of Terrestrial Laser Scanning (TLS) (Seymour et al., 2018), a portable ground-based LiDAR device. This technology reduces costs compared with traditional LiDAR surveys by eliminating the need for crewed aircrafts, thus enabling higher frequency surveys to be performed. This technology, however, has its own limitations, including a high capital investment and significant human effort to perform a survey (Westoby et al., 2012). They are also restricted to line of sight from the device, requiring multiple laser deployments to cover an area. These requirements, combined with the high amount of human effort, typically limits the mapping area of TLS devices to 0.05 km^2 or less (Seymour et al., 2018). In the field of coastal sciences this prevents surveying at municipal scales, which includes beaches, estuaries, and dunes that can extend many kilometres (Seymour et al., 2018).

Another popular modelling technique in coastal science is Real-Time Kinematic Global Navigation Satellite Systems (RTK-GNSS) (Drummond et al., 2015), which is a handheld GPS device that measures single point coordinates and elevation. Traditional techniques include walking the device along a transect to produce a 2-dimensionl profile, or combining multiple transects and points to interpolate a 3-dimensional surface (Drummond et al., 2015). Compared with LiDAR and TLS, RTK-GNSS provides a more accessible platform in terms of cost and portability. The main detraction is the low resolution for 3-dimensional modelling, determined by how closely spaced transects and points are, leading to uncertain DEMs from interpolation errors (Drummond et al., 2015). Increasing the resolution involves exponentially more human effort and it is impossible to attain resolution as good as TLS/LiDAR. Additionally, due to the need for physical access, this technique can be destructive to fragile ecosystems and access can be prevented by dense or sensitive vegetation.

The limitations of both LiDAR/TLS and RTK-GNSS technologies, has created a technological gap for drone technology (Klemas, 2015). While having drastically lower

costs than TLS, drones are capable of producing similar DEMs while enabling a faster data acquisition that can often be automated and on a larger scale (Seymour et al., 2018). However, for airborne LiDAR, a similar spatial scale is not yet achievable by drones although technological advancements, particularly with fixed wing drones and emerging battery technology, is presenting promising survey extensions (Seymour et al., 2018). The main advantage of drone approaches over LiDAR is the ability to perform surveys more frequently due to lower costs, and less logistical planning (Klemas, 2015). Increasing the density of surveys over time enables a better understanding of the dynamic processes within the coastal environment (Mancini et al., 2013). While drone technology has successfully been applied to small scale coastal studies (Seymour et al., 2018), the potential of the technology to coastal research has still not been fully realised (Drummond et al., 2015).

2.2.4 Application of Drones to Oyster Reefs

While the understanding of drone technology is growing, the application to oyster reefs is still largely unexplored. Modelling of oyster reefs in the past has mainly used TLS technology, such as that featured in research by Rodriguez et al. (2014) and Ridge et al. (2017) for analysing the growth rate of individual reefs. This approach has only been successful in modelling individual reefs while presenting complications for incorporating the surrounding sediment substrate due to survey area limitations, as described in section 2.2.3. Past research that incorporates the surrounding substrate has been completed using RTK-GNSS survey techniques. Past research by Walles et al. (2015) used this method by taking single points every 2 – 4 m on and around each oyster reef to interpolate a topographic surface. Another study by Strachan (2019) modelled an oyster reef and sediment substrate by measuring multiple transects on and around the reef to model the 3-dimensional surface. Complications in the RTK-GNSS methodology stem from often sparse and irregular data coverage which results in large errors from the interpolation process (Drummond et al., 2015). Drones have the

potential to overcome the complications of these past methods and is the aim of this thesis to explore its potential application in the hydrodynamic study of oyster reefs.

3 Study Area

To fulfill the aims and objectives of this thesis, an oyster reef in Port Hacking, New South Wales (NSW), Australia, was chosen as the study site (34°4'24.79" S, 151°7' 14.56" E). The site is located on the east coast of Australia, approximately 36 km south of the Sydney Harbour entrance (Figure 3.1). This reef is of interest as it is the site of ongoing collaborative research from the Sydney Institute of Marine Science (SIMS) with various Sydney based universities. Such research has focused on the biological and physical processes of oyster reefs, with a combined goal of understanding and maximising the benefits from oyster reefs.

Figure 3.1. Anticlockwise from the top left. A map of Australia illustrating the location of the Port Hacking Estuary. A satellite image map of the greater Sydney region, with an extent indicator of the right map. A satellite image of the Port Hacking Estuary identifying the oyster reef study site from the estuary mouth. All base map hybrid imagery sources: Esri, DigitalGlobe, GeoEye, i-cubed, USDA FSA, USGS, AEX, Getmapping, Aerogrid, IGN, IGP, swisstopo, and the GIS User Community.

3.1 Physical Context

The Port Hacking estuary is located in the southern outskirts of Sydney, separating the heavily populated Sydney suburbs to the North from the relatively untouched Royal National Park to the south (Figure 3.1). Its formation, as with other NSW east coast estuaries, began from rising sea levels that drowned river valleys and low lying coastal areas during the Post Glacial Marine Transgression (Roy et al., 2001). For Port Hacking, this occurred in the drowned Hacking River valley, incised into Middle Triassic Sandstone (Roy, 1994). As sea-level rise stabilised about 6.5 thousand years ago (ka) (Roy, 1994), sediment from terrestrial and oceanic sources infilled to establish the Port Hacking estuary (Albani and Cotis, 2007). The sediment composition is predominantly sand throughout the main channel, with smaller bays and arms filled with muddy-sand, and mud (Albani and Cotis, 2007).

3.2 Hydrodynamics

The estuary is tide dominated and microtidal with a range of 0.2 - 1.9 m. Freshwater inputs to the estuary come from the Hacking River, which predominantly runs through the Royal National Park to the south (Figure 3.2). The catchment area is 165 km^2, generating a low fluvial input with an estimated deposition of 1-2 mm per year (Kench, 1999). Saline marine waters come from the South Pacific Ocean to the east, relying on tides, wind and ocean swell for mixing. The oceanic swell regime is predominantly from the south-southeast (146.25°-168.74°TN), accounting for 29.5% of the annual wave direction from March 1992 – March 2013 (Kulmar et al., 2013) (Figure 3.3). The entrance to the estuary is protected by multiple headlands and the Deban Spit (Figure 3.1), however significant storm events can penetrate into the estuary causing large sand depositions, helping facilitate a net upstream sediment transport (Albani and Cotis, 2007).

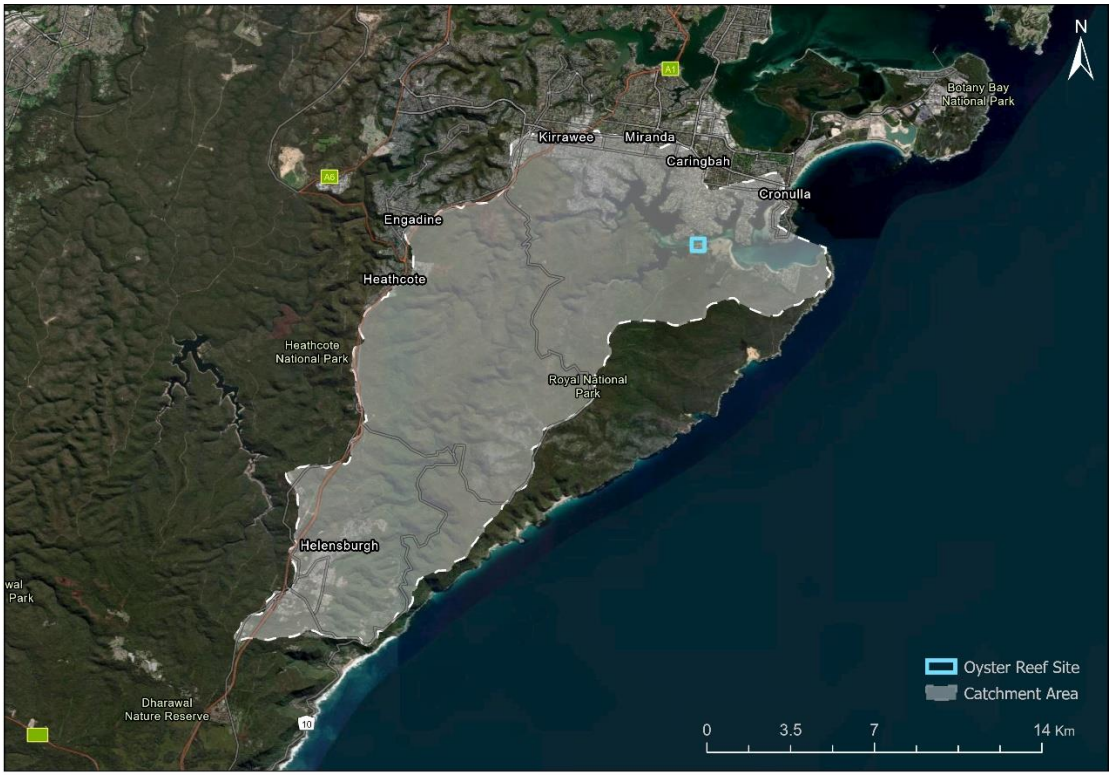

Figure 3.2. The catchment area of the Port Hacking river and oyster reef location. Base map hybrid imagery sources: Esri, DigitalGlobe, GeoEye, i-cubed, USDA FSA, USGS, AEX, Getmapping, Aerogrid, IGN, IGP, swisstopo, and the GIS User Community.

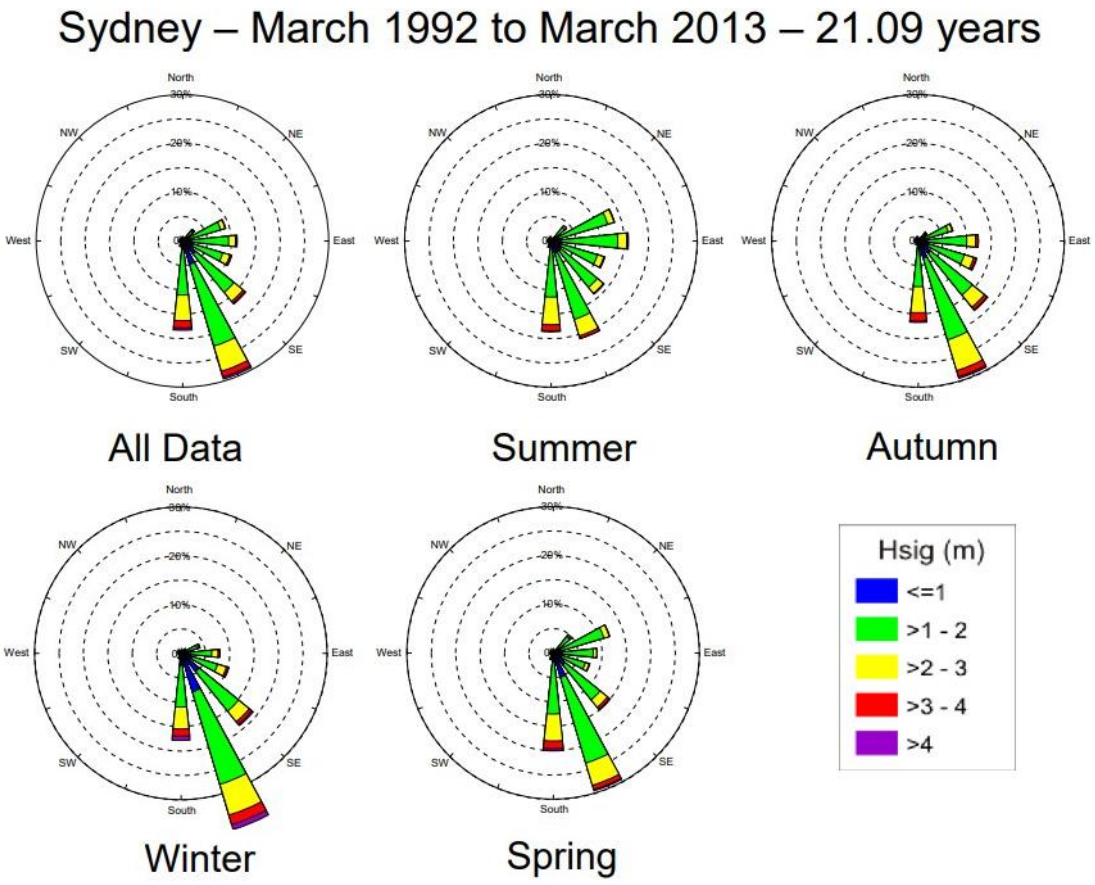

Figure 3.3. The seasonal wave climate of Sydney illustrating direction and significant wave height (H_s). Original figures were produced by Kulmar et al. (2013) based off data collected by the Manly Hydraulics Laboratory (MHL) Sydney Waverider buoy between March 1992 to March 2013.

3.3 History of Human Impacts

The first signs of human activity occurred some 8000 years ago in Port Hacking, but debate around prior activity is still ongoing (Albani and Cotis, 2007). To the aboriginals that occupied this area, the estuary was known as Djeebahn. Their unobtrusive impacts on the estuary were halted after the first fleeter Henry Hacking encountered the estuary in 1788, renaming it as Port Hacking, with the subsequent spread of settlement to the foreshores and headwaters. The earliest exploitation of the estuary was for fishing operations, recorded as early as 1806 where 660 kg of fish were caught and shipped to Sydney (Albani and Cotis, 2007). As commercial operations continued, the estuary eventually became a marine reserve in 1880 as fish populations were dwindling. Physical changes to the estuary have been recorded as early as the 1840s with the

commencement of shell grit mining operations (Albani and Cotis, 2007), the process of extracting shell fragments the sediment substrate for lime production. The demand of lime for the building and construction industry lead to this being the longest lasting industry in Port Hacking. The 1880s saw further alteration to the physical environment from dredging operations to maintain navigation channels. These operations are still ongoing, but with a focus on maintaining channels for the use of recreational boaters. These immense physical changes have altered the development and health of the Port Hacking estuary, and while a focus towards restoration has ensued, the estuary is far from the conditions it once was.

3.4 Oyster Reefs

The origins of the Port Hacking oyster reef stem from the shell grit mining operations that occurred in the estuary during the 1850s. Small vessels would unload sandstone blocks, used as ballast weights, and replace them with shell grit and timber. Sometime after gritting operations ceased in the 1850s, oysters naturally began to grow over the sandstone blocks, giving its current name ‘The Ballast Heap’. Overexploitation of oysters in Port Hacking occurred as early as 1885, when the southern shore was declared an oyster reserve as it was threatened with extinction from gathering and farming operations. To help rectify this, live oysters were imported from America in 1886 to advance the recovery efforts (Albani and Cotis, 2007). Oyster farming operations did continue on a small scale in Port Hacking, with commercial operations continuing as late as the 1970s (Albani and Cotis, 2007). No formal oyster farming operations have occurred since.

3.5 Past Research at Port Hacking

The Sydney Harbour Research Program (SHRP), a collaborative research program part of the Sydney Institute of Marine Science (SIMS), has focused on studying the characteristics of sediments around oyster reefs, with study sites in the Port Hacking

and Hunter estuaries. Of relevance from this initiative is the recent thesis by Strachan (2019), which explored the biodeposition of trace metals and wave attenuation. Her study found that oyster reefs dissipate wave energy, causing a sediment accumulation on the leeward side of the reef. This project hopes to further elaborate on this research through a spatial analysis of the sediment accumulation patterns, and their relationships to oyster reef hydrodynamics.

4 Methodology

This chapter outlines the methods undertaken to meet the aims and objectives of this project. Data was acquired from 3 fieldwork campaigns detailed in Section 4.1. Data processing was divided into two sections, the first (Section 4.2) outlines the processing of topographic data for DEM generation. And the second (Section 4.3) outlines the processing of environmental data sets to understand the hydrodynamic conditions at the Port Hacking oyster reef. The different environmental and topographic data collection and field campaigns is visualised in Figure 4.1 for better understanding.

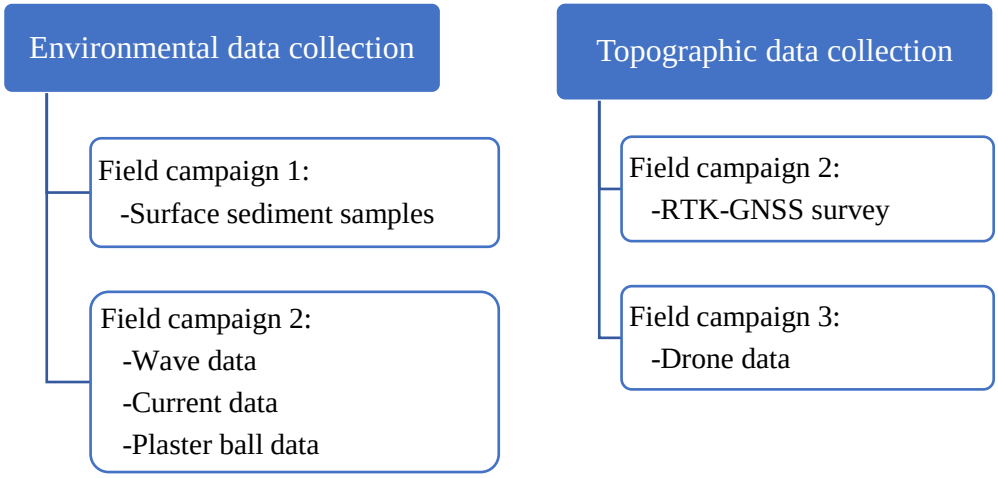

Figure 4.1. Illustration of how the different field campaigns and data types were used for either environmental or topographic analysis.

4.1 Data Acquisition

The data used for this project was acquired during 3 fieldwork campaigns at the Port Hacking oyster reef, detailed in the following subsections. The first was completed on the 23rd of October 2018, collecting surface sediments for grainsize analysis (Subsection 4.1.1), the second was on the 24th to 25th of October 2019, collecting hydrodynamic and elevation data (Subsection 4.1.2), and the third on the 10th of March 2020, collecting photogrammetric data for DEM generation (Subsection 4.1.3).

4.1.1 First Fieldwork Campaign

Sediment surface samples were collected on the 23rd of October 2018, with a total of 60 samples collected, to analyse the sediment characteristics and their spatial trends around the reef. Sampling involved taking sand from the top 0-2cm of surface sediment, in a random cloud arrangement around the reef and at varying distances from the reef. Three reference samples were collected, each 200m from the reef with two in the leeward direction, and 1 on the channel side. The location of each sample was identified using an RTK-GNSS, see Figure 4.2. Samples were collected in plastic centrifuge tubes, transported on ice and frozen in the lab to preserve any organic content.

Figure 4.2. Surface sediment samples taken around the Port Hacking oyster reef in Oct '18. Geocentric Datum of Australia (GDA94) coordinate system utilised. Base map hybrid imagery sources: Esri, DigitalGlobe, GeoEye, i-cubed, USDA FSA, USGS, AEX, Getmapping, Aerogrid, IGN, IGP, swisstopo, and the GIS User Community.

4.1.2 Second Fieldwork Campaign

The second field campaign aimed to collect data for investigating the hydrodynamic conditions that vary spatially around the oyster reef. This included the deployment of pressure transducers to record wave data, current meters to record water velocity, as

well as plaster balls that identify relative hydrodynamic energy changes. The deployments occurred over a 24-hour period, from the 24th to 25th of October 2019. This campaign also included RTK-GNSS data collection for DEM generation (Figure 4.3).

A total of 6 pressure transducers (Aquistar PT2X) and 2 current meters (Nortek Vectors) were deployed (Figure 4.4). These pressure transducers are devices that convert pressure changes in the water column to electrical signals, which based on the signal strength and time between signal spikes can identify parameters of passing waves. The pressure transducers used in this project recorded at 4 Hz. The current meters are devices that record the flow of water in the X and Y horizontal directions, which enable an analysis of the currents and how they change over time. The current meters used were recorded at 16 Hz. The first current meter was deployed at 0.14 m above the sediment substrate, and current meter 2 at 0.21 m. Pressure transducer #6 (PT6) was deployed at 3cm above the sediment substrate, PT8 at 6 cm, PT11 at 4cm, PT15 at 2.3 cm, PT16 at 1.3 cm, and PT17 at 3 cm. The location of each instrument was measured using an RTK-GNSS (Figure 4.3).

The method of deploying multiple plaster balls within an area uses the premise that individual balls will erode relative to the hydrodynamic energy they are placed in, where more energy equates to a higher weight loss in the ball (Yokoyama et al., 2004). During this field campaign plaster balls were deployed around the Port Hacking oyster reef for 24 hours, from the 24th to 25th of October 2019, with a total 50 balls deployed at random locations around the reef. The spherical engineered plaster balls were attached to metal rods that were used to suspend the balls above the sediment substrate, with a mean height of 2.2 cm above the substrate (Figure 4.4). The location of each ball was recorded using an RTK-GNSS (Figure 4.3). The dry weight of the ball was taken before and after deployment.

An RTK-GNSS elevation survey was completed over the two days using a grid like pattern to maintain an even coverage of points over the area. Coordinates were collected

using a Trimble R8 RTK-GNSS mounted to a 2 m carbon fibre pole, with a positional accuracy of 8mm horizontally and 15 mm vertically. Points were recorded in GDA 94 (Geocentric Datum of Australia) zone 56 coordinates, and heights were recorded with respect to AHD (Australian Height Datum), a datum surface based off 30 tide gauges around Australia to estimate a zero mean sea level (MSL). Points were recorded every 5 seconds while walking the handheld RTK-GNSS at a consistent pace in a gridded pattern on and around the reef (Figure 4.3), collecting a total of 7,829 points.

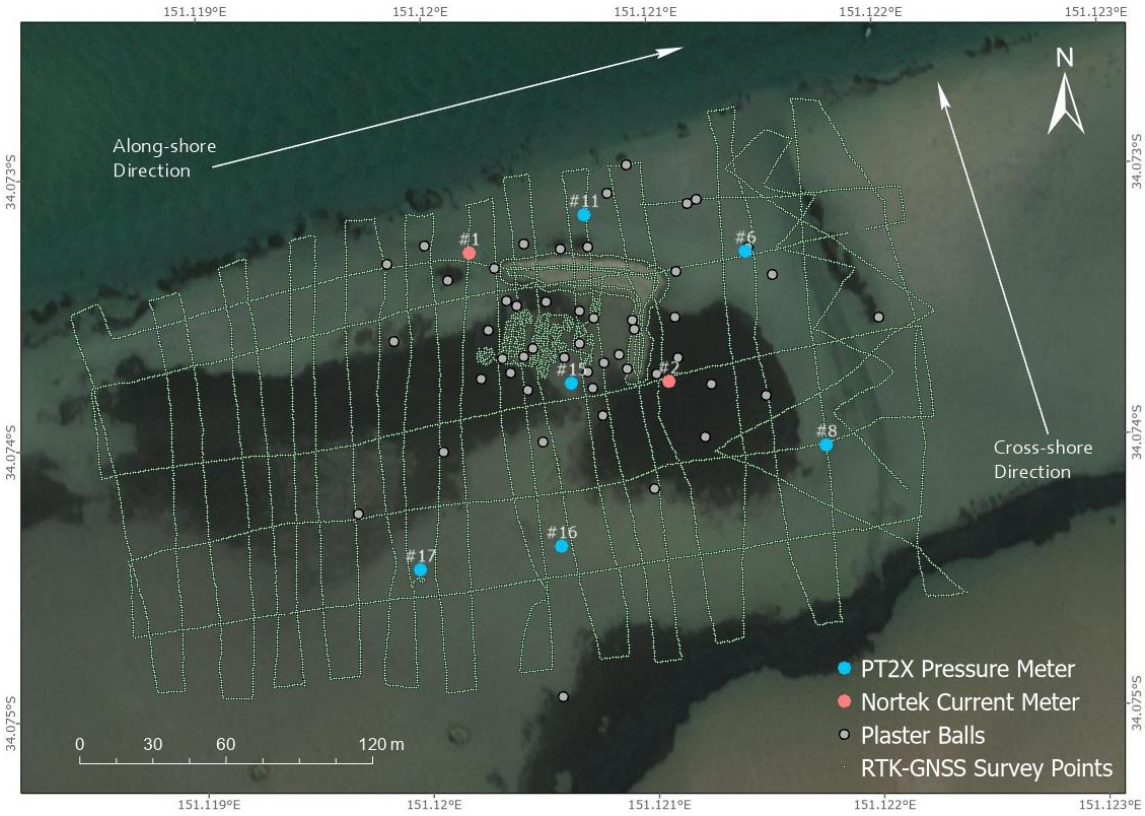

Figure 4.3. Plaster ball, pressure transducer, and current meter locations around the Port Hacking oyster reef during field work on 24th to 25th Oct 2019. Positive cross-shore and along-shore current directions from the main channel are illustrated. Label numbers are the pressure/current meter device identification numbers used during analysis. Green points identify the elevation point locations of the RTK-GNSS survey. Base map hybrid imagery sources: Esri, DigitalGlobe, GeoEye, i-cubed, USDA FSA, USGS, AEX, Getmapping, Aerogrid, IGN, IGP, swisstopo, and the GIS User Community.

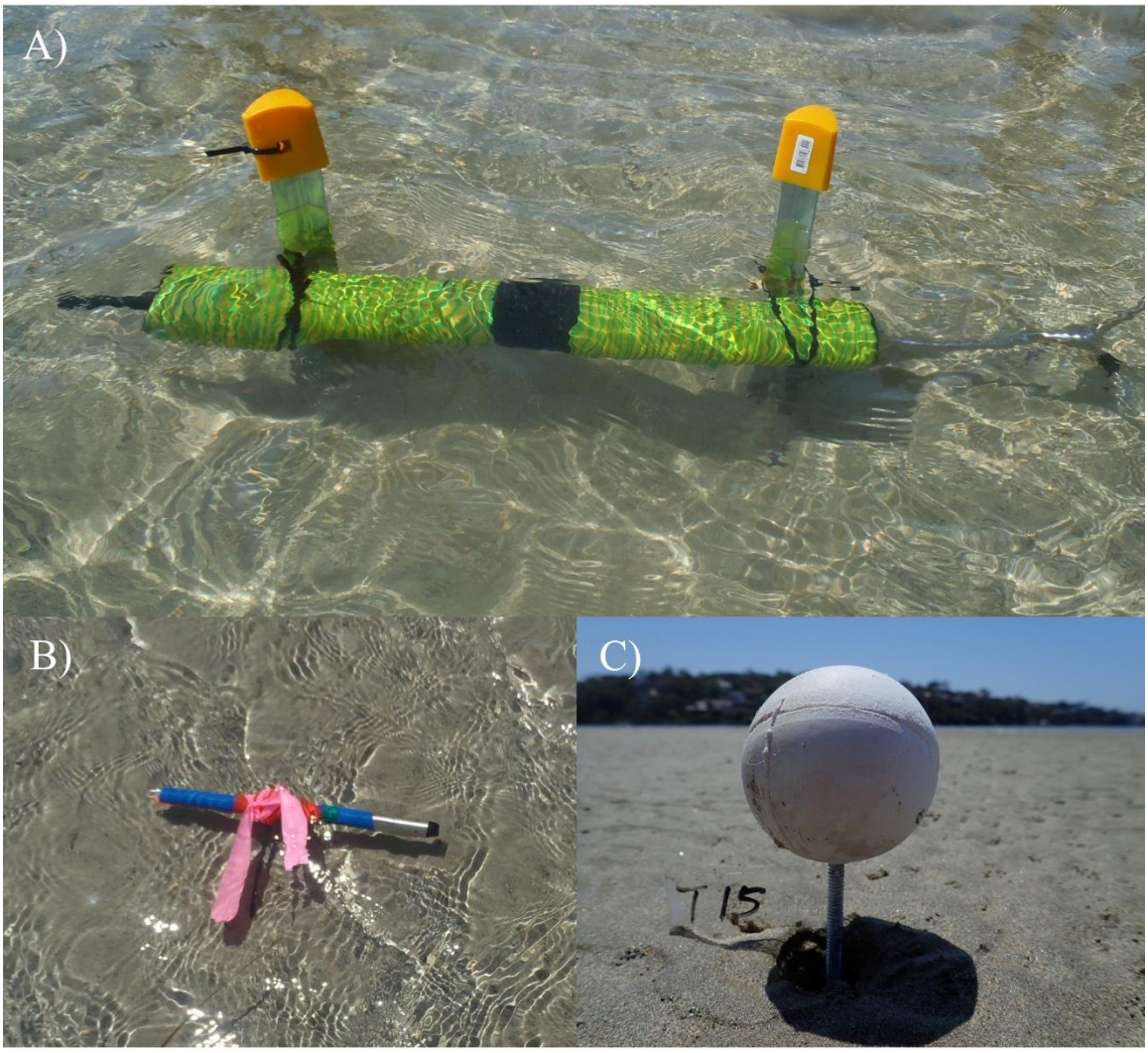

Figure 4.4. Deployment of the Nortek Vector current meter (A), the Aquistar PT2X pressure transducer (B), and plaster ball (C) during field work on the 24th of October 2019 at the Port Hacking oyster reef.

4.1.3 Third Field Campaign

Fieldwork for this campaign consisted of a photogrammetric survey of the oyster reef. This is the processes of obtaining geometric information of physical objects and the environment from a series of overlapping photographs and GCPs. Imagery was obtained using a DJI Phantom Pro 4 drone, and GCPs using a Trimble R8 RTK-GNSS. The total survey area incorporated the reef and sediment substrate surrounding (Figure 4.5). As the survey area alternates between being submerged and exposed during the tidal cycle, a spring peak low tide of 0.05 m was identified on the 10th of March 2020, at 4:26pm (AEST) for maximum substrate exposure.

GCPs were accurately measured to spatially orient the photogrammetric model. GCPs used were marked using A4 sized targets, with a 2x2 grid pattern of opposite yellow/black squares (Figure 4.6). The layout of the GCPs was along the edges of the survey area and stratigraphically distributed throughout (Figure 4.5), as outlined by Martínez-Carricondo et al. (2018) to maximise accuracy. Coordinates were taken at the centre of each marker using a Trimble R8 RTK-GNSS mounted to a 2 m carbon fibre pole, with a positional accuracy of 8mm horizontally and 15 mm vertically. Points were recorded in GDA 94 zone 56 coordinates, and heights above AHD.

For an accurate photogrammetric model, certain flight parameters must be obtained during the aerial survey. This includes the image overlap, and camera gimbal angle. The software to create the model, Agisoft Metashape Professional, outlines recommended values of 80% side and 70% front image overlap, 70° gimbal angle and a minimum single point coverage of 5 images (LCC, 2019). The front image overlap identifies how often an image is taken along the flight path based on the drone speed and camera field of view. The side image overlap determines the spacing between the flight paths over the study area to ensure the images along each path overlaps with the previous path by 80%.

There are also physical and technological limitations that dictate how the aerial survey is performed. The first is flight time. Based on the drone model and number of batteries, the flight must be safely within the total flight time available. This must factor in time and distance to return to the starting point for battery changes, as well as a safety margin as changes in weather conditions may affect the drones flight efficiency, such as changes in wind speed and/or direction (Joyce et al., 2019). The second consideration is the resolution required for the data analysis. For increased resolution, the drone must be flown at lower elevations from the ground surface. The general flight path for a survey is a grid where the drone will fly in an ‘S’ like manner back and forth along grid lines. The complication with this is that lower altitudes results in a narrower image coverage,

and so to achieve the required image overlap the drone flight path must be a tighter grid, which takes a longer time. Balancing the resolution requirements with technological limitations is key to planning a successful survey.

For this survey, the total area survey was a 373 x 290 m grid (Figure 4.5). The drone was a DJI Phantom Pro 4, with 3 batteries giving a total safe flight time of 1hr 15mins. Flight planning for the highest possible resolution resulted in a 27 m altitude minimum and a 59 min survey time, with an additional 5 mins allocated to each battery to return to the starting point for landing and battery changes.

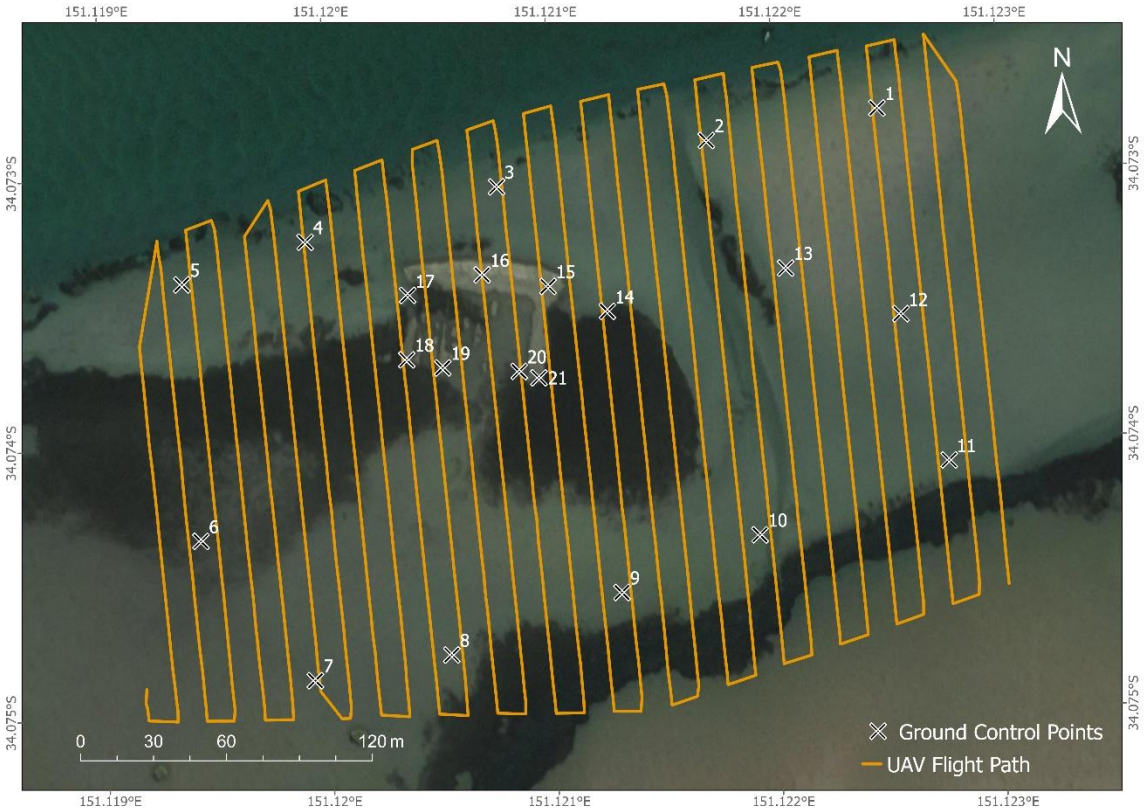

Figure 4.5. Drone (DJI Phantom Pro 4) flight path performed during aerial image data collection. Total flight time was 59 mins including 3 battery changes. Take-off/landing site was to the east of the study area. GCP locations are marked by crosses around the perimeter of the survey and stratigraphically throughout. Base map hybrid imagery sources: Esri, DigitalGlobe, GeoEye, i-cubed, USDA FSA, USGS, AEX, Getmapping, Aerogrid, IGN, IGP, swisstopo, and the GIS User Community.

Figure 4.6. Field work photos taken during the drone survey. A) Aerial image of the Port Hacking Reef taken from 120m altitude looking away from the estuary opening towards the West-Southwest. B) GCP marker #21 placed on top of the reef. C) Measuring coordinates of GCP markers using the RTK-GNSS on the sediment substrate surrounding the reef.

4.2 Topographic Data Processing

Two DEMs were created from different data types and methods; the first an interpolated model from the RTK-GNSS survey points, and the second a photogrammetric technique from the drone survey and GCPs. The two methods for DEM generation are explained in the following subsections 4.2.1, and 4.2.2. A final subsection, 4.2.3, outlines how the two models were compared.

4.2.1 RTK-GNSS Digital Elevation Model

A DEM from the RTK-GNSS data obtained in the second campaign (Section 4.1.2) was created using kriging interpolation from the survey points. A total of 7,829 points were used with a simple kriging interpolation method, using a spherical semi-variogram model with a variable search radius of 25 points. The optimal search radius was determined by cross-validation to the original points to minimise the mean square error value.

4.2.2 Photogrammetric Digital Elevation Model

Generation of the photogrammetric DEM was achieved using the data collected in the drone and GCP survey and processed using *Agisoft Metashape Professional* software (see Appendix 9.1 for complete software processing parameters). The processes of creating the DEM starts by uploading geotagged images from the drone and performing a photo alignment, which compares and matches pixels between different images to estimate the camera locations of each image and 3-dimensional location of matched pixels. This process results in a sparse point cloud. GCP markers are then identified in the images and camera alignment re-run to optimise their location with spatial references. Any low-quality images, or images with a high reconstruction uncertainty are automatically removed. As the sparse cloud only contains a small fraction of total points identified, the next process is to build the full dense cloud. This process spatially orientates each matched image pixel with an x/y/z location. A DEM is additionally generated from the dense point cloud data, where the resolution of the output is determined by the effective ground resolution of the dense point cloud (LCC, 2019), and cell values calculated using an inverse distance weighted interpolation. Additional data exports include an orthomosaic of the survey area based on the geometric properties of the DEM.

To identify the accuracy of the photogrammetric model the discrepancies between the RTK-GNSS collected GCPs and dense point cloud were evaluated. This was done by

comparing the distances between each GCP and the corresponding cloud point, and calculating the route mean square error (RMSE) of the results. To further investigate the accuracy and errors of the model the distances were broken down into X (easting), Y (northing), and Z (altitude) domains, and an RMSE was calculated for each domain. As the dense point cloud was the highest resolution dataset produced, the error results of this dataset were used for the total accuracy of photogrammetric processing.

Analysis of the DEM was performed to identify morphological patterns of the sediment substrate surrounding the oyster reef, with elevation contours identified for 1 cm increments around the reef. An adaptive smoothing algorithm was applied to contour lines to remove the jagged and angular appearance of some artefacts, commonly associated with high resolution DEMs (Gonçalves and Henriques, 2015). This process allows a more general analysis of surface elevation trends, enabling the visualisation of the sediment accumulation patterns across the survey area. The algorithm used by this project, defined by (Bodansky et al., 2001), is a Polynomial Approximation with Exponential Kernel (PAEK), which uses a parametric continuous averaging technique to smooth line features. This was performed using ArcGIS Pro (Version 2.6.1) with a default smoothing tolerance value of 2.5, where a lower number would reduce the smoothing effect and higher would increase smoothing. Additionally, the algorithm modifies its affect based on the slope, where a reduced smoothing occurs in areas of increased slope to preserve physiographic features and increases smoothing in flatter areas.

4.2.3 Comparing Digital Elevation Models

To identify the morphological changes between the RTK-GNSS and drone surveys, points from the RTK-GNSS survey were identified with the corresponding cell of the drone DEM and the difference calculated to identify elevation changes between the two models. A statistical spatial analysis was then performed to identify the trends of these

value differences, as well as interpolated into a surface to spatially analyse the morphological changes of the sediment substrate around the oyster reef. The interpolated surface was also produced using a simple kriging method with identical parameters as listed above in section 4.2.1. Data processing and interpolation was completed using ArcGIS Pro (ver 2.6.1).

4.3 Environmental Data Processing

The following subsections outline the processing of various datasets obtained from all three field campaigns (Sections 4.1.1, 4.1.2, and 4.1.3) that were used to infer the hydrodynamic conditions in the study area.

4.3.1 Wind, Oceanic Swell, and Tide Data

Wind and tide data were obtained for the 24th to 25th of October 2019 field campaign from nearby weather stations. Wind data, 10 min mean wind speed, was collected from the nearest Bureau Of Meteorology (BOM) weather station, located at Kurnell (-34.0039, 151.2111, station number 066043). Oceanic wave data was collected from the Sydney offshore wave data buoy (station code WAVESYD) operated by Manly Hydraulics Laboratory (MHL) at approximated 44 km northeast from our study area. Wave data included hourly records for significant wave height (H_s - average height of the top 33% of waves), maximum wave height (Hmax), mean period (Tz), and wave direction (deg TN). These data sets were utilised in the analysis of observed data to identify relationships, or aid in the analysis. The wind and oceanic swell data were used to identify the source of waves experienced by the reef (Subsection 4.3.2), and tide data used to confirm tidal cycles and heights controlling observed current strengths (Subsection 4.3.2).

4.3.2 Wave and Current Data

Data processing of the pressure transducer included detrending of mean water level to remove the tide signal. A Spectral wave analysis was utilised to separate and analyse waves of different periods. This included two spectrums: sea-swell waves, and infragravity waves. Sea-swell spectrum waves are wind generated waves, defined by waves less than 20 seconds in period, while infragravity spectrum waves are surface gravity waves that have a period higher than sea-swell, between 20 seconds and 3 minutes 20 seconds. Each wave spectrum was then analysed for wave parameters of Hs (mean height of the highest 33% of waves) and T_z (peak period associated with the maximum energy in the spectrum). Parameters for infragravity waves were calculated using a wave-by-wave analysis, where gravity waves were isolated using a high-pass filter and infragravity waves using a low-pass filter. All processing was completed using MATLAB (ver. R2020a).

Current meter data was processed to identify the intensity and direction of currents experienced by the reef. Data was analysed in the X/Y domain relative to the main channel, where X was cross-shore and Y along-shore direction (Figure 4.3). The Nortek current meter also outputs a correlation value, which is the normalised amplitude of the auto-correlation function. These values were used to apply a noise filter, where values below a correlation threshold of 90% were replaced with data points of the moving average. All data processing was completed using MATLAB (ver. R2020a).

As the reef and surrounding sediment substrate is exposed during low tides, data analysis was confined to times when all pressure transducers or meters were completely submerged. Therefore, gaps in the data exist during the lows of tidal cycles.

4.3.3 Sediment Grainsize

Grainsize analysis was performed using a Malvern Mastersizer 2000 laser particle size analyser. For surface sediments, samples were divided into 4 equal subsamples and analysed individually. Pre-treatment of subsamples included the removal of organic

matter by using hydrogen peroxide (H_2O_2) and a hot water bath for 24 hrs. Clay aggregates were removed using a Calgon solution that disperses aggregates and spun for 24hrs in a centrifuge to separate and then remove. The grainsize analysis took the average size distribution from a triplicate of measurements for each subsample. Results were given as a percentage within size classes, starting at 1.48×10^{-6} mm and increasing by 0.148% of the previous class up to a maximum grainsize of 10 mm (see Appendix 9.2). Summary of samples were given as the 10th percentile (D_{10}), 50th percentile or median (D_{50}) and 90th percentile (D_{90}). Grainsize sorting was calculated as the absolute deviation from the median. This was calculated using the following equation.

$$Sorting = \frac{\sum V_i |D_{50} - D_i|}{D_{50} \sum V_i}$$

$$D_{50} = Median\ grainsize$$

$$D_i = Diamater\ of\ size\ class$$

$$V_i = Volume\ in\ size\ class$$

A high sorting value indicates poorly sorted sediment, and a low value well sorted. Results were mapped using ArcGIS Pro (ver. 2.5.1) with graduated point size and colours to identify spatial distributions.

4.3.4 Plaster Ball Data

To analyse the plaster ball data, the mass changes of each ball was converted to percentages of their original weight to give a relative change between balls. Spatial analysis of the balls was performed in ArcGIS Pro (ver. 2.5.1), using the RTK-GNSS points of each ball. Graduated symbology, based on mass percentage change, was used to visualise spatial trends of relative hydrodynamic energy around the reef.

5 Results

5.1 Topographic data

The following subsections detail the results and analysis of the two different DEMs. The first subsection (5.1.1) is the DEM created using interpolated RTK-GNSS survey points from the second field campaign. The second subsection (5.1.2) is the DEM developed using drone data from the third field campaign with photogrammetric techniques. A comparison between the two DEMs is presented in section 5.1.2 to explore how the surface has changed over time.

5.1.1 RTK-GNSS Digital Elevation Model

From the RTK-GNSS survey in the second field campaign (Subsection 4.1.2) 7,829 points were used in a kriging interpolation. The resulting raster comprised 374 columns by 251 rows, with a square cell size of 0.98 m, giving a coverage area of 367.9 m by 246.9 m, and a total area of 90,834 m^2. Total data point density is 1 point per 11.6 m^2. The minimum cell values are -1.08 m, a maximum of 0.4 m, and a mean of -0.43 m ± 0.21 m standard deviation (SD). Visual analysis of the DEM (Figure 5.1) revealed some of the main morphological features also present in the drone DEM, including the main reef and smaller reef sections inside clearly visible as the highest elevation areas. The main channel to the north of the reef, and secondary channel to east, are both clearly visible depressions. The secondary channel running across the southeast corner is visible as a depression feature but lacks detail due to few sampling points taken on either side of the channel (Figure 4.3). An increased elevation area to the southeast of the reef, similarly identified in the drone DEM (Figure 5.2), is also visible. The size of this area, however, appears to extend further towards the southeast, with a notable expansion of the shadow towards the perimeter of survey area. This area was not covered in the drone survey and so not possible for comparison.

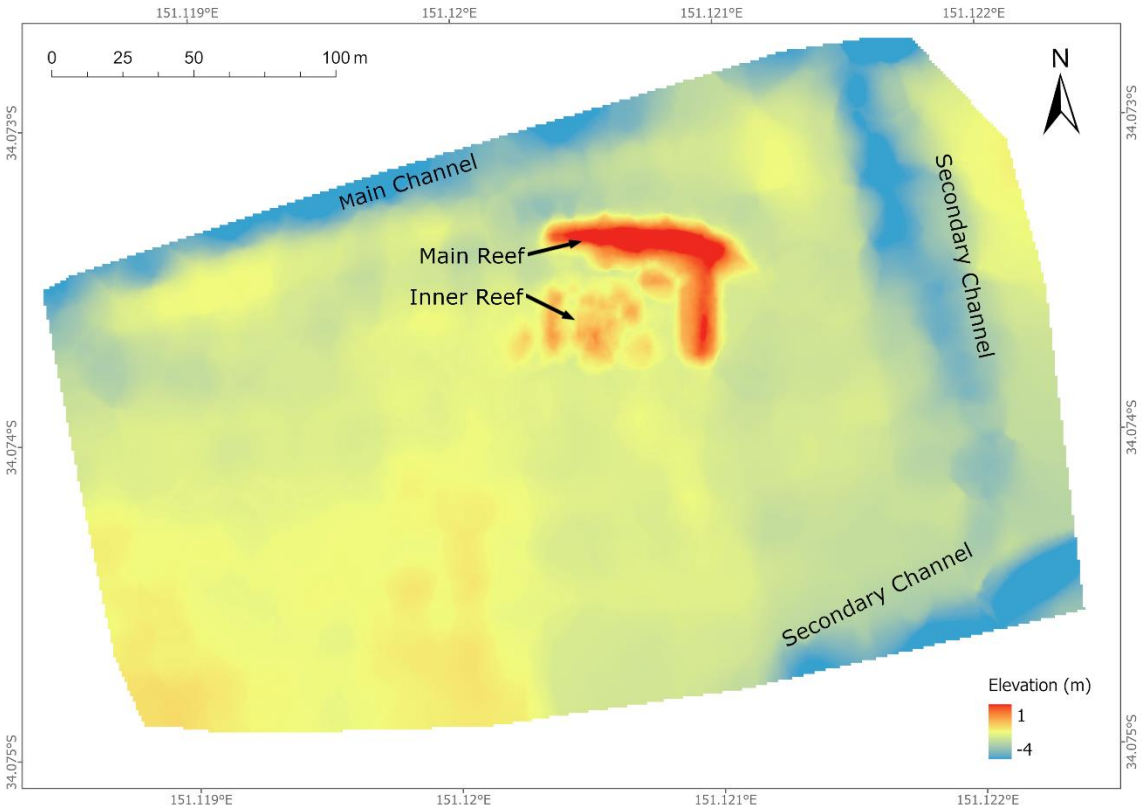

Figure 5.1. Interpolated DEM from RTK-GNSS survey data of the Port Hacking oyster reef and surrounding sediment substrate. Elevation values are using the AHD (Australian Height Datum) with mean sea level (MSL) at zero metres.

5.1.2 Photogrammetric Digital Elevation Model

From the drone flight, a total of 1,292 images were included, resulting in 2,379,261 tie points between images. 21 GCPs were incorporated, with each one being identified in an average of 13.19 images. The dense point cloud produced a total of 113,315,226 points. The resulting DEM has a square pixel size of 2.86 cm with a total dimension of 517 x 409 m. The calculated errors associated with photogrammetric processing are summarised in Table 5.1, with a total RMS error of 3.64 cm. A trend of high vertical errors occurred at GCPs 15 to 17, which together create a parallel transect over the largest and only alongshore trending section of reef (Figure 4.5). No error trends or anomalies were observed in the horizontal (X/Y) domains.

Table 5.1. The distances (error) between the RTK-GNSS measured GCPs and corresponding dense point cloud value. Errors were explored in the X, Y, and Z domains, as well as total (XYZ). The last column is the number of images where each GCP marker was identified. See figure 4.5.3.a for GCP locations

GCP	X error (cm)	Y error (cm)	Z error (cm)	Total XYZ Error (cm)	# of Images GCP identified in
1	-0.58	0.77	-1.42	1.71	14
2	-0.76	-0.65	3.81	3.94	15
3	-0.26	-0.31	4.96	4.97	13
4	-1.63	0.54	2.84	3.32	12
5	-0.36	-0.03	-1.58	1.62	14
6	-0.59	-0.45	-1.04	1.28	12
7	-0.75	1.48	-0.30	1.69	15
8	0.58	0.24	1.70	1.81	14
9	-0.52	0.84	1.90	2.14	14
10	0.67	-0.09	1.53	1.67	12
11	0.21	0.24	-1.27	1.31	14
12	-0.15	-0.70	-1.02	1.24	8
13	0.07	-1.04	-0.22	1.07	14
14	1.97	0.05	3.00	3.59	14
15	0.44	0.65	-6.80	6.84	13
16	-0.05	0.97	-8.29	8.34	12
17	0.45	-1.34	5.69	5.86	13
18	0.32	-0.85	-3.00	3.13	14
19	0.20	0.24	-1.15	1.19	15
20	0.04	-0.60	3.67	3.72	12
21	0.75	0.06	-3.63	3.71	13
Total RMSE	**0.72**	**0.71**	**3.50**	**3.64**	**13.19**

Illustrations of the orthomosaic and DEM are in Figure 5.2. The main channel to the north of the reef, smaller parallel secondary channel to the south, and perpendicular secondary channel joining the two to the east, are clearly visible as low elevation zones below sea level. Drainage patterns are also present over the sediment substrate surrounding the reef, particularly from the northeast corner of the main reef feeding into the main channel (Figure 5.2.B). This is also linked to the large depression along the channel side of the main reef, feeding into the main channel. The regions of seagrass, visible in the orthomosaic (Figure 5.2.A), also appear on the DEM with visible distinctions along the northern and eastern boundaries of seagrass. The seagrass elevation remains slightly higher than surrounding areas with a more gradual and less

distinct transition back to sand along the southwestern boundaries. Similar patterns also exist with two sand banks that appear along the main channel, indicated as orange zones (Figure 5.2), where a more distinct boundary on the north-eastern side compared to a gradual transition in the south/southeast.

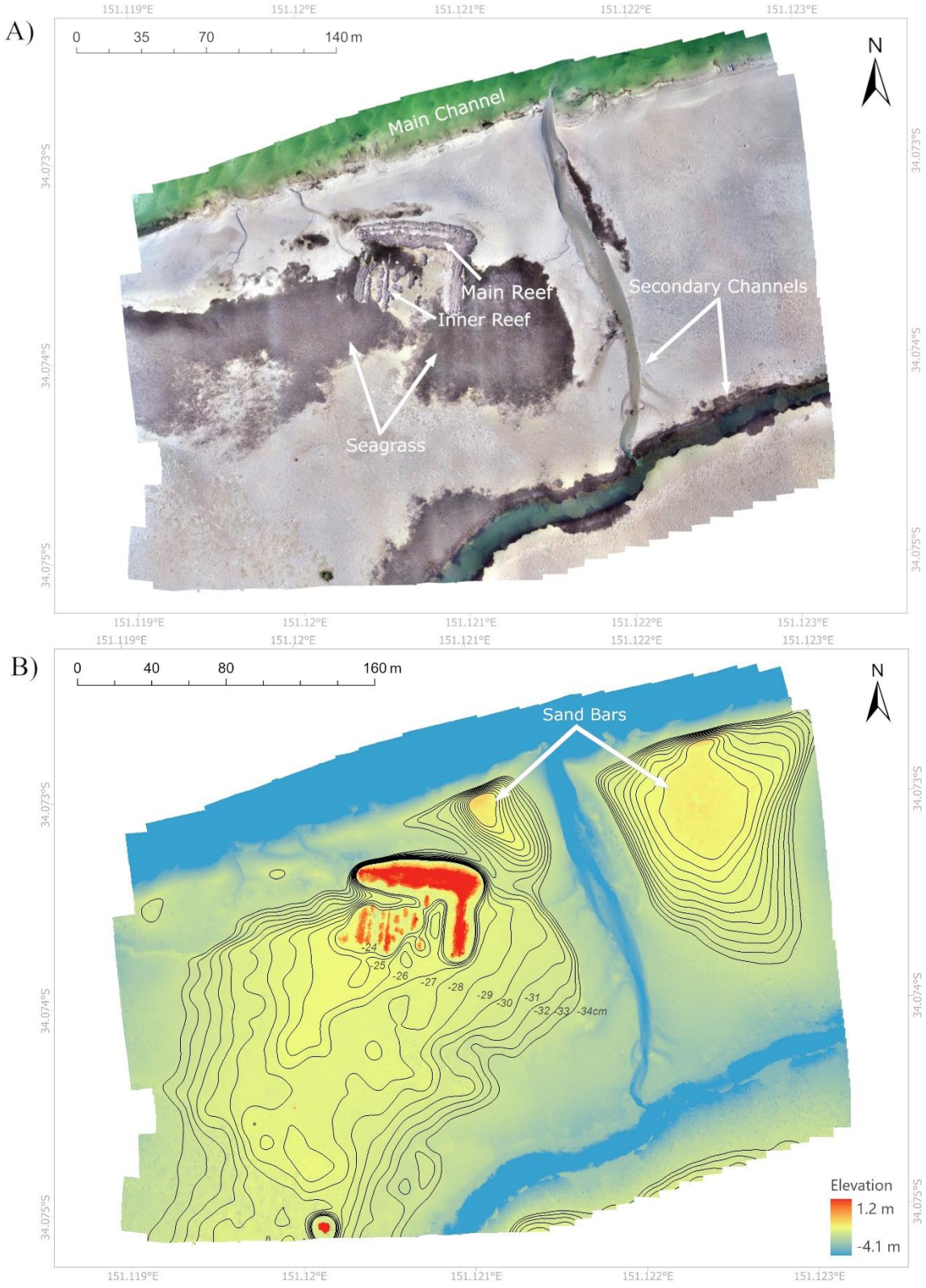

Figure 5.2. Image A) is the orthophoto mosaic output from the drone survey with annotations of morphological features. Image B) is the DEM output with elevation contours of the sediment substrate around the Port Hacking oyster reef. Contours are at 1 cm intervals from -34 cm up to -24 cm (MSL), to illustrate sediment accumulation patterns around the reef.

An elevation contour analysis of the substrate surrounding the reef gives an insight to the sediment accumulation patterns. Figure 5.2.B illustrates 1 cm interval smoothed contours from -34 cm up to -24 cm mean sea level (MSL), generated from the drone DEM. The contour trends reveal a steeper gradient along the northern boundary of the main oyster reef, mean gradient of 4.34%, towards the main estuarine channel. An inverse trend is observed in the opposite south-southeast direction where terrain is much flatter with a 0.01% gradient. These trends are similarly observed in two other sand banks located to the north, in front of the reef, and to the northwest on the opposite side of the channel. The extent of these two banks are however considerably smaller than that of the oyster reef, with a steeper gradient observed in the leeward direction, 0.2% for the bank to the north and 0.14% for the bank on the opposite side of the channel. These results suggest that although shallow gradients exist away from the main channel, those behind the reef are much shallower and an elevation zone extends much farther, indicating that sediment accumulates in the leeward direction behind the reef more significantly than a natural sand bar.

To identify changes in the sediment substrate overtime, the difference between the RTK-GNSS points and corresponding point in the drone dense point cloud were calculated and results interpolated into a surface (Figure 5.3). The most notable trend was an increase in elevation around the reef, indicating accretion of sediment, while moving away from the reef and outside the shadow we notice a decrease, or erosion. To summarise these changes, the -30 cm contour line from Figure 5.2.B was used to statistically compare the difference from inside and outside the sediment accumulation area, also only including points on the sediment substrate and not on the reef. Points located within the -30 cm shadow had a mean accretion of 1.0 cm, while outside of this area the mean change was -2.0 cm. In considering the vertical accuracy of the RTK-GNSS device (0.15 cm) and the vertical errors of the drone DEM (3.64 cm), the 3.0 cm difference between the two areas is not possible to confirm a significant difference as the total error is greater than the difference found. This highlights that although a net

sediment accretion appears to occur in the leeward direction from the reef, the difference is not significant enough to overcome possible errors associated with data processing and device accuracy.

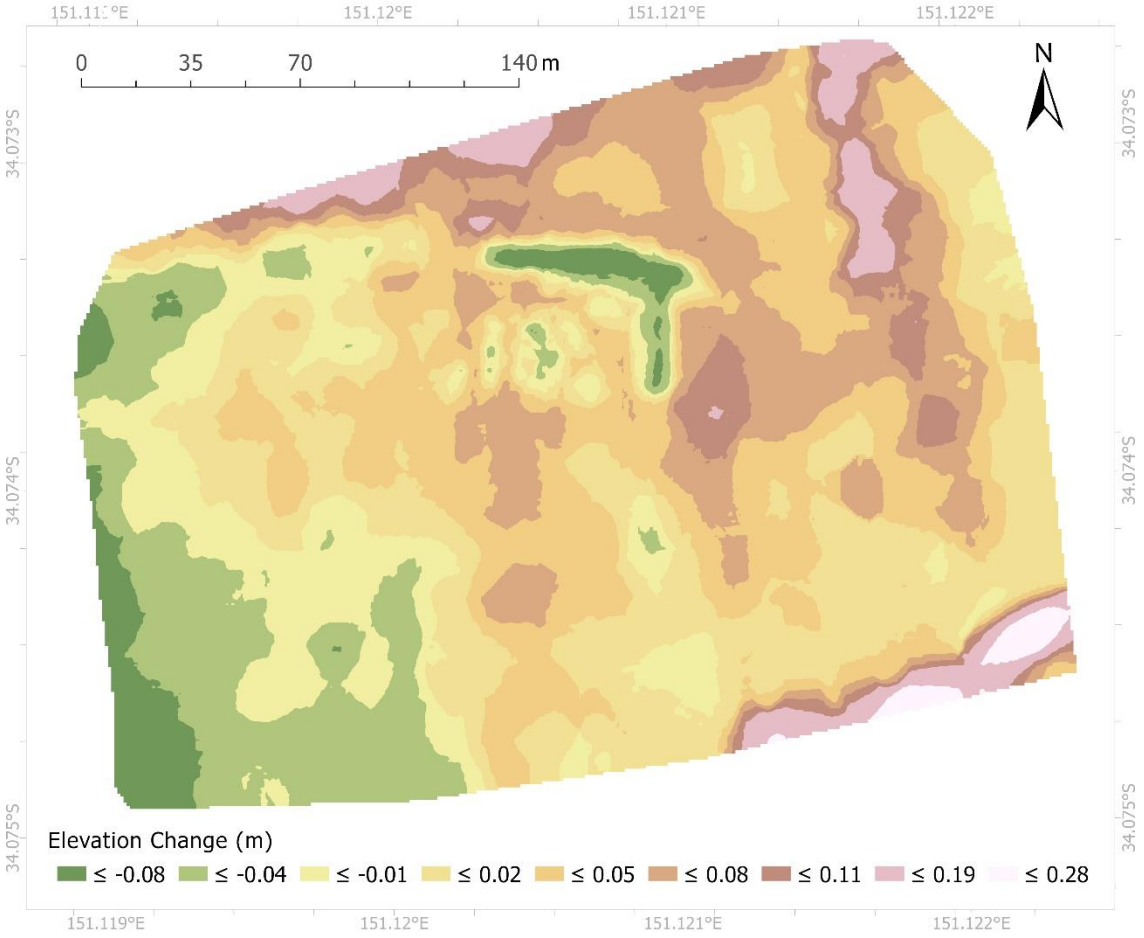

Figure 5.3. Changes in elevation between RTK-GNSS points (24th-25th Oct 2019) and drone DEM (10th Mar 2020), illustrating accumulation or erosion of sediment over time.

5.2 Environmental Data

The following sections explore the various results from processing environmental data, collectively contributing to understanding the hydrodynamic conditions experienced by the Port Hacking oyster reef and answering the first research aim; do oyster reefs control local hydrodynamics? Figure 5.4 illustrates the locations of all environmental data analysed.

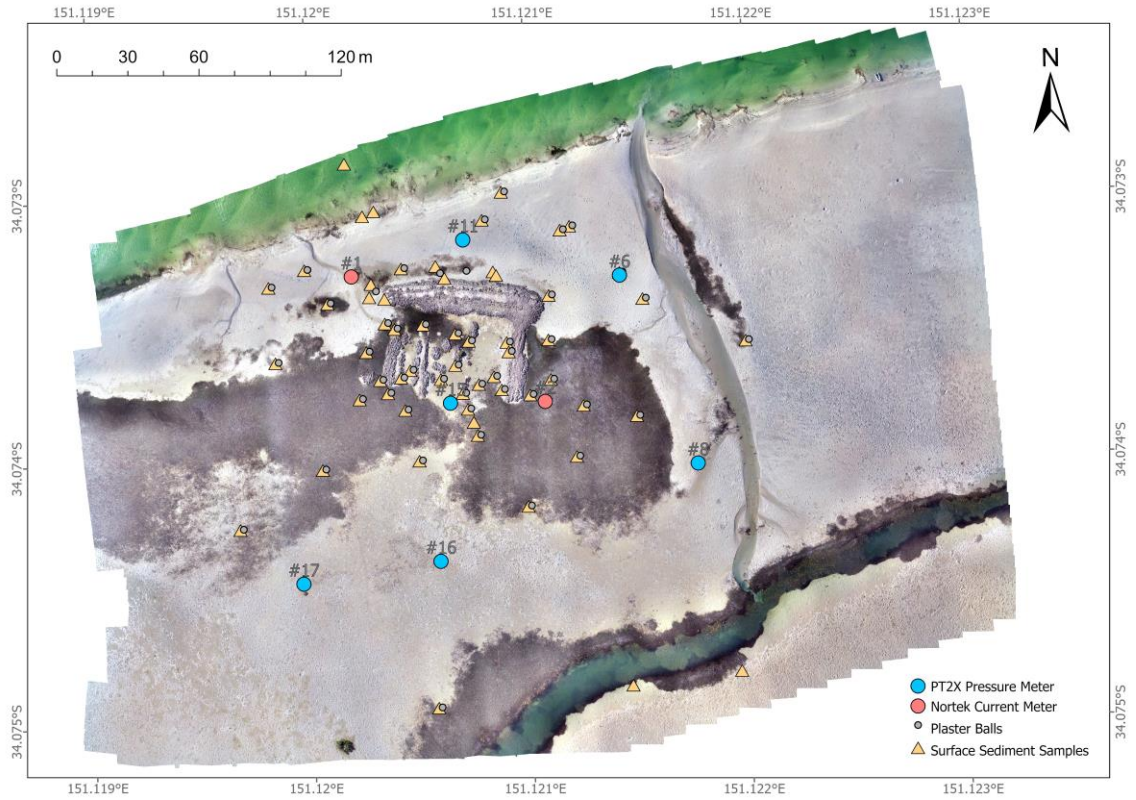

Figure 5.4. Location of all devices and samples included in the analysis of environmental data.

5.2.1 Wind and Oceanic Swell

Oceanic swell data for the second campaign (24th to 25th of October 2019) identified a generally decreasing H_s trend in the ocean waves, from 0.98 m to 0.78 m, until 05:00 on the 25th where H_s starts increasing. This increase in swell coincided with a progressive change in swell direction from east-southeast to the northeast (Figure 5.5). Wind conditions during this time were also from the east-southeast on the 24th, with a change in direction to the north-northwest at around 3am on the 25th. Wind speed fluctuated mostly between 10 and 20 km/h on the 24th, with a decrease occurring over the hour leading up to the direction change. Once the direction changed, wind speeds remained between 10 and 20 km/h until a noticeable increase to over 20 km/h after 09:00.

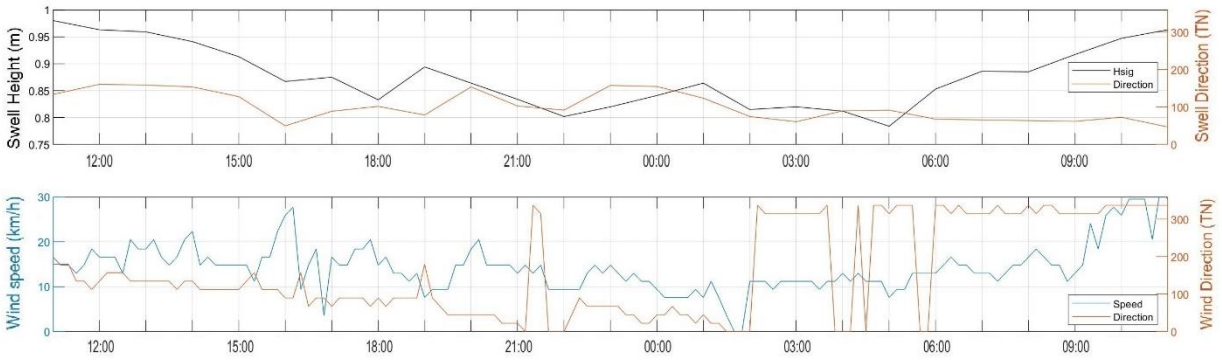

Figure 5.5. Top graph is the oceanic swell height (black) graphed against direction (red) from the 24th and 25th of October 2019. Data was recorded at the Sydney Waverider buoy, and made available from the Manly Hydraulics Laboratory (MHL). The lower graph is a plot of wind speed and direction during the same time, with data from the Kurnell weather station, made available from the Bureau of Meteorology, Australia.

5.2.2 Sea-Swell Waves

During the 24hr field survey, two periods were identified during which all 6 pressure transducers (PT) were submerged. The first was a high-high tide between 12:30 and 22:30 on the 24th October 2019 (1.58 m), and a low-high between 03:00 and 10:30 on the 25th October 2019 (1.36 m). A summary of the mean significant wave height (H_s) for each transducer, tidal cycle, and ebb/flood phase is summarised in Table 5.2, and the time series is plotted in Figure 5.6. Overall, we observed very small wave conditions, mostly less than 2 cm in height. The source of waves experienced by the reef was explored using a correlation analysis to local wind and ocean swell data from Section 5.2.1. We observed a moderate to strong positive correlation to the two most exposed pressure transducers on the channel side of the reef. The correlation coefficent for PT11 and PT6 was 0.51 and 0.46 respectivley. No significant correlation to ocean swell data was observed, indicating that the source of waves experienced by the reef was from local wind, occuring from a NW to NE direction during the observation period.

In comparing the spatial relationship between the transducer results, we can observe a trend in reducing wave heights as we move away from the main channel. PT11 and PT6, located closest to the channel (Figure 4.4), experienced the greatest H_s (mean of 1.3 cm for both), with heights significantly ($P<0.05$) greater than all other transducers

except for PT17. Both locations also experienced very similar wave heights regardless of tidal phase (Table 5.2). This was also the case for PT8 and PT16, both a similar distance from the main channel and with very similar recordings regardless of tidal phase (Table 5.2). The transducer furthest from the reef, PT17, did not follow a similar trend of decreasing wave height from the channel (Figure 5.6). At a similar distance from the channel as PT16 and PT8, it had a significantly ($P<0.05$) greater H_s and was instead much closer to PT11 and PT6, on the channel side of the reef, with no significant difference. The location of this transducer as the farthest from the reef, as well as furthest alongshore from the reef (Figure 4.4), suggests that the decrease in wave energy at other locations is from their proximity to the reef, and as we move further away from the reef that influence diminishes.

Table 5.2. Mean H_s during the first and second tidal cycles, as well as further divided into flood and ebb periods of each cycle. Results are in centre meters (cm) ± standard deviation (SD), and ordered by distance from the main channel, closest first.

Pressure Transducer	Tide 1 (cm)	Tide 2 (cm)	Tide 1 Flood (cm)	Tide 2 Flood (cm)	Tide 1 Ebb (cm)	Tide 2 Ebb (cm)
11	1.7 ± 0.5	0.8 ± 0.7	1.9 ± 0.5	0.3 ± 0.2	1.4 ± 0.4	1.4 ± 0.4
6	1.7 ± 0.3	0.9 ± 0.6	1.7 ± 0.3	0.3 ± 0.2	1.7 ± 0.3	1.4 ± 0.4
15	0.9 ± 0.6	0.4 ± 0.3	0.9 ± 0.6	0.2 ± 0.1	0.9 ± 0.6	0.6 ± 0.3
8	1.1 ± 0.2	0.8 ± 0.2	1.1 ± 0.3	0.6 ± 0.1	1.1 ± 0.2	1.0 ± 0.1
16	1.1 ± 0.3	0.7 ± 0.3	1.1 ± 0.3	0.5 ± 0.1	1.0 ± 0.2	1.0 ± 0.1
17	1.3 ± 0.5	0.9 ± 0.3	1.3 ± 0.5	0.7 ± 0.2	1.3 ± 0.4	1.2 ± 0.2

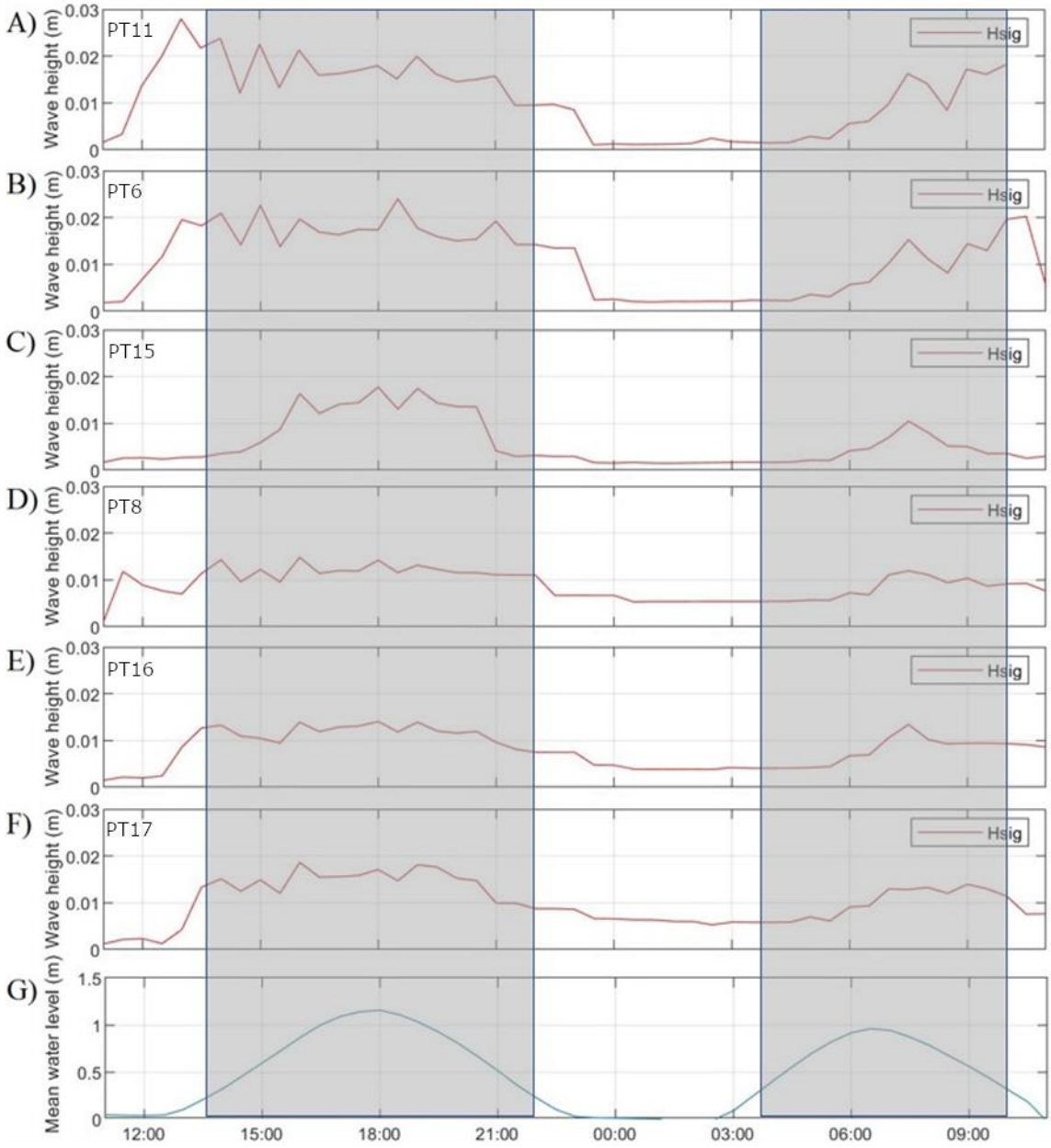

Figure 5.6. Significant wave height results from the wave spectral analysis of 6 pressure transducers (PT) around the Port Hacking oyster reef. Results are listed by PT distance from the main channel, closest first. A) PT-11, B) PT-6, C) PT-15 D) PT-8 E) PT-16 F) PT-17 G) Recorded mean water level. Grey zones indicate the times when all PT's were completely submerged in water.

Data trends revealed much lower wave heights for PT15 located on the inside of the reef, which was significantly ($P<0.05$) less than all other transducers. When looking at the plots of PT15 (Figure 5.6) we can also observe a shorter window of wave heights experienced during each tidal cycle, where an increase in wave height was observed only at much higher tide heights than all other transducers. To further investigate this, H_s was analysed during both tidal cycles when mean water level was above 0.8 m. In

comparison to PT11, located on the opposite channel side of the reef, we observe no significant difference when water level is over 0.8 m, but while below 0.8m the difference was significant. This suggests that waves were only able to reach PT15 during high tides, possibly when the reef is completely submerged and waves able to pass over the reef from the main channel. Mean wave heights while above 0.8 m was 1.45 cm for PT15 and 1.71 cm for PT11. To further explore the propagation of waves over the reef during this high tide period PT16 was also analysed, which between the 3 transducers creates a north-south trending transect over the reef with relatively even spacings (Figure 4.3). This resulted in a linear decline in wave height with 1.32 cm recorded for PT16 (Figure 5.7). PT6 and PT8 were similarly analysed, which together created a similar north-south transect but that does not pass over the reef. This transect identified a similar but slightly steeper decline in wave height with distance from the main channel. These transects suggest that the influence of the reef for wave dissipation is reduced during high tide, and that during these tidal phase's dissipation is more influenced by distance from the channel.

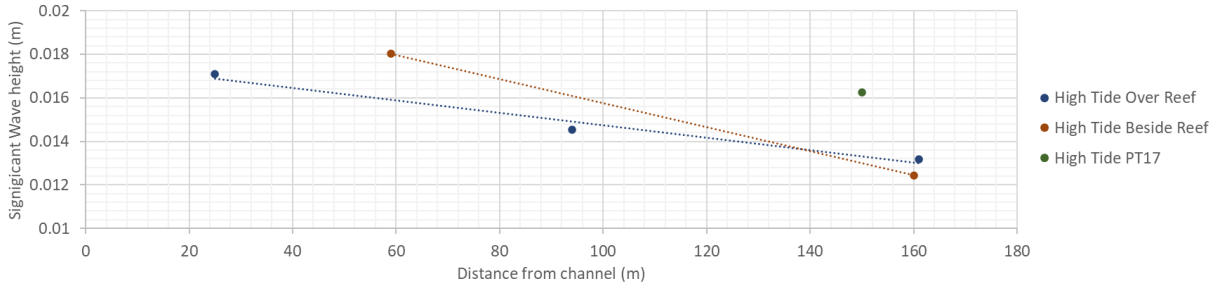

Figure 5.7. Wave dissipation analysis from the main channel during high tides (water level recorded above 0.8 m). Transect points over the reef include fore-reef (PT11), inner reef (PT15) and behind reef (PT16). Transect beside reef includes transducer PT6 and PT8. Trend line over the reef identified a 3 mm H_s drop per 100 m over the reef, and 6 mm per 100 m beside the reef.

An analysis of wave period for the sea-swell wave spectrum was also completed to further investigate the wave conditions experienced by the reef. The results, shown in Figure 5.8, found similar patterns in wave periods over time between all transducer locations. A statistical analysis of results, looking for significant difference between transducers, only found one instance of significant difference for PT15. This

significance found that during the first tidal cycle PT15 was significantly greater than all other transducers. No other incidents of significant difference between transducers during different tidal cycles were identified, suggesting a strong similarity between results regardless of location. Overall trends illustrate an increasing wave period during the first tidal cycle, with two spikes at 17:30 and 20:00. The second tidal cycle revealed a slight decreasing trend with a small spike present in the final reading at 10:30. These results suggest that wave period was mostly similar amongst all transducers, with recordings of very short period swell (between 1 and 4 s) likely from local wind sources.

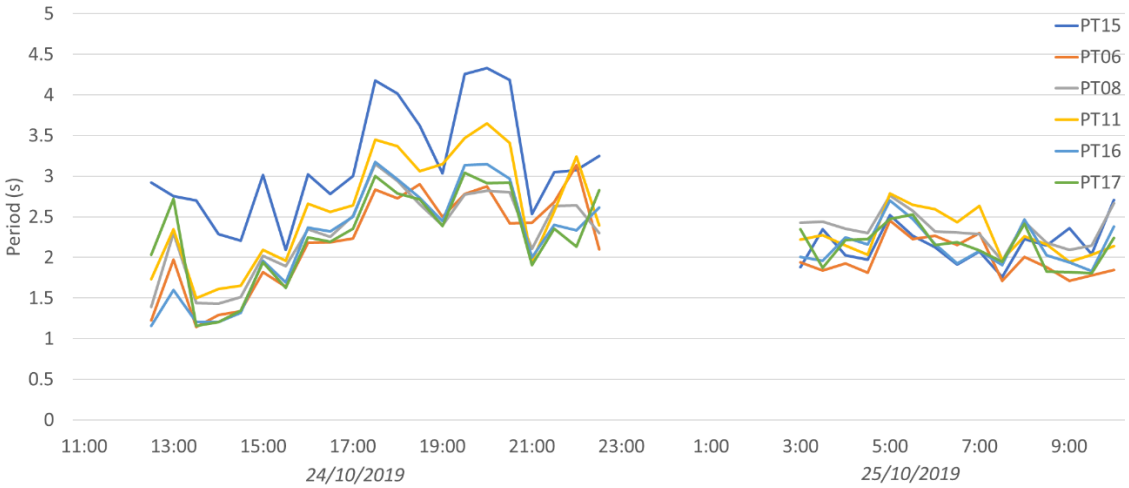

Figure 5.8. Sea-swell wave period recorded by pressure transducers during the 24th – 25th October 2019 field campaign. Gaps in recordings are due to the transducers being exposed during low tides.

5.2.3 Infragravity Waves

Infragravity waves were identified similarly to sea-swell waves, separating waves in the infragravity band of 0.005 - 0.05 Hz, or a period of 200 to 20 seconds. The infragravity results of each transducer is illustrated in Figure 5.9. Overall, we observed very small infragravity waves, in the range of 2 – 5 mm. Spatial trends of results revealed an increasing wave height moving away from the main channel, however no significant difference was observed ($P<0.05$). This result is opposite to sea-swell waves which indicated a decreasing wave height away from the channel. To further compare the sea-

swell and infragravity results, the same high tide analysis of water levels above 0.8 m was performed on infragravity waves, results shown in Figure 5.10. This analysis revealed a linear increase in infragravity Hs moving away from the channel and over the reef, and the transect beside the reef revealed a slightly larger increase in H_s. These trends over and beside the reef are the inverse of sea-swell waves, suggesting that a relationship may exist between H_s wave height changes between the two wave spectral bands.

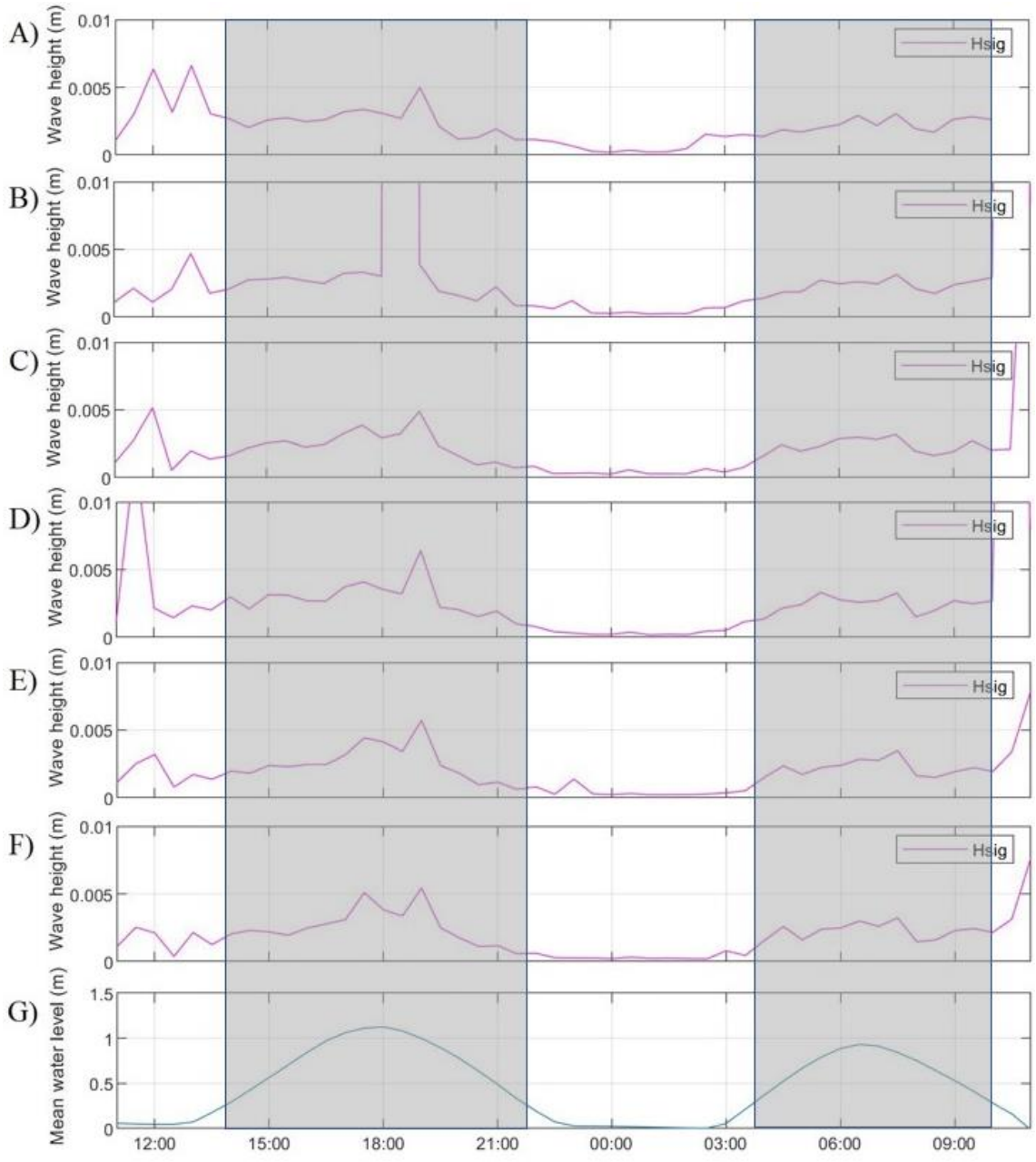

Figure 5.9. Infragravity significant wave height results from the wave spectral analysis of 6 pressure transducers (PT) around the Port Hacking oyster reef. Results are listed by PT distance from the main channel, closest first. A) PT-11, B) PT-6, C) PT-15 D) PT-8 E) PT-16 F) PT-17 G) Recorded mean water level. Grey zones indicate the times when all PT's were completely submerged in water.

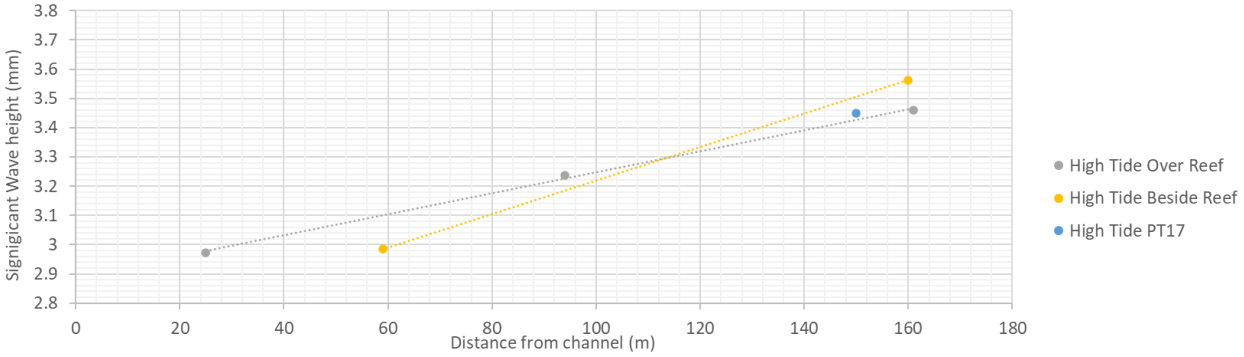

Figure 5.10. Infragravity wave dissipation analysis from the main channel during high tides (water level recorded above 0.8 m). Transect points over the reef include fore-reef (PT11), inner reef (PT15) and behind reef (PT16). Transect beside reef includes transducer PT6 and PT8. Trend line over the reef identified a 0.57 mm Hs drop per 100m, and a 0.36 mm drop per 100 m drop beside the reef.

Wave period was also observed for the infragravity waves to further illustrate the wave conditions experienced by the reef, results plotted in Figure 5.11. Data trends during the recording period revealed similar peaks and troughs between all transducers. There was no significant difference between transducers during the recording period, or during each tidal cycle. Overall, we see quite high variation in period from a minimum recorded value of 51 s up to a maximum of 255 s. The second tidal cycle was notably lower than the first, which was similarly illustrated in H_s. The very small height of such infragravity waves suggests that they are of such little energy to concern the morphological development of the sediment substrate but are none the less a source of hydrodynamic energy experienced by the reef.

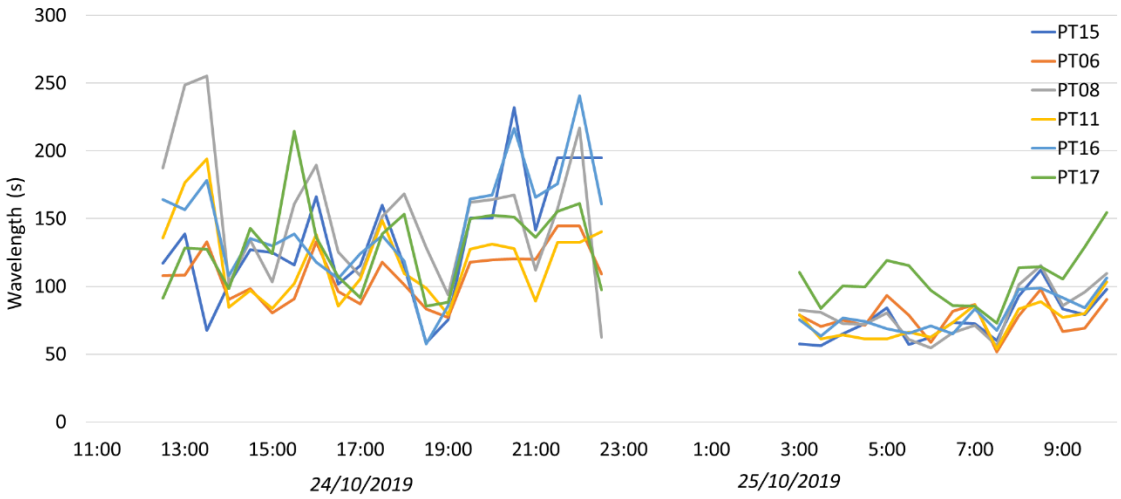

Figure 5.11. Infragravity wave period recorded by pressure transducers during the 24th – 25th October 2019 field campaign. Gaps in recordings are due to the transducers being exposed during low tides.

5.2.4 Current Strength and Direction

The 24-hr deployment of two current meters recorded two tidal cycles, with observations between 14:00 to 22:00 on the 24th, and 04:00 to 10:30 on the 25th. General data trends revealed a much stronger cross-shore current than alongshore, regardless of location or flood and ebb tidal phases. Current meter 2, located in in seagrass to the east of the reef and less exposed (Figure 4.3), experienced slightly higher mean currents than current meter 1 to the magnitude of 6.7% greater during the flood phase, and 8.3% during ebb (Table 5.3). Both locations identified predominantly cross-shore currents, with current meter 1's direction during flood phase averaging 189.7° from the positive cross-shore direction, and 9.6° for the ebb. Current meter 2 illustrated a slightly more cross-shore dominant direction with 181.8° during the flood phase, and 3.1° during ebb. The flood tide phase identified stronger currents than the ebb phase, with current meter 1 and 2 recording 40.5% (3.8 cm/s) and 38.5% (3.5 cm/s) stronger currents, respectively. The direction and greater strength of the flood tides both agree with the sediment contours observed around the reef in section 5.1.1, where the stronger currents towards the south-southeast direction contribute to a net sediment transport mechanism in this direction.

Table 5.3: Mean current strength (cm/s) in cross-shore/alongshore (X/Y) and total (XY) strength for two current meters deployed on the Port Hacking oyster reef. Results were broken down into the two tidal cycles observed, as well as the ebb and flood phases.

Current Meter/ Direction	**Flood Mean (cm/s)**	**Ebb Mean (cm/s)**	**Tide 1 Flood (cm/s)**	**Tide 2 Flood (cm/s)**	**Tide 1 Ebb (cm/s)**	**Tide 2 Ebb (cm/s)**
Current Meter 1						
Cross-shore (X)	-11.6	8.3	-11.5	-11.8	8.6	7.9
Alongshore (Y)	-2.0	1.4	-1.9	-2.1	1.4	1.4
Total Direction (XY)	-11.8	8.4	-11.6	-12.0	8.7	8.1
Current Meter 2						
Cross-shore (X)	-12.6	9.1	-12.0	-13.3	9.0	9.2
Alongshore (Y)	-0.4	0.5	-0.4	-0.4	0.5	0.5
Total Direction (XY)	-12.6	9.1	-12.0	-13.3	9.0	9.2

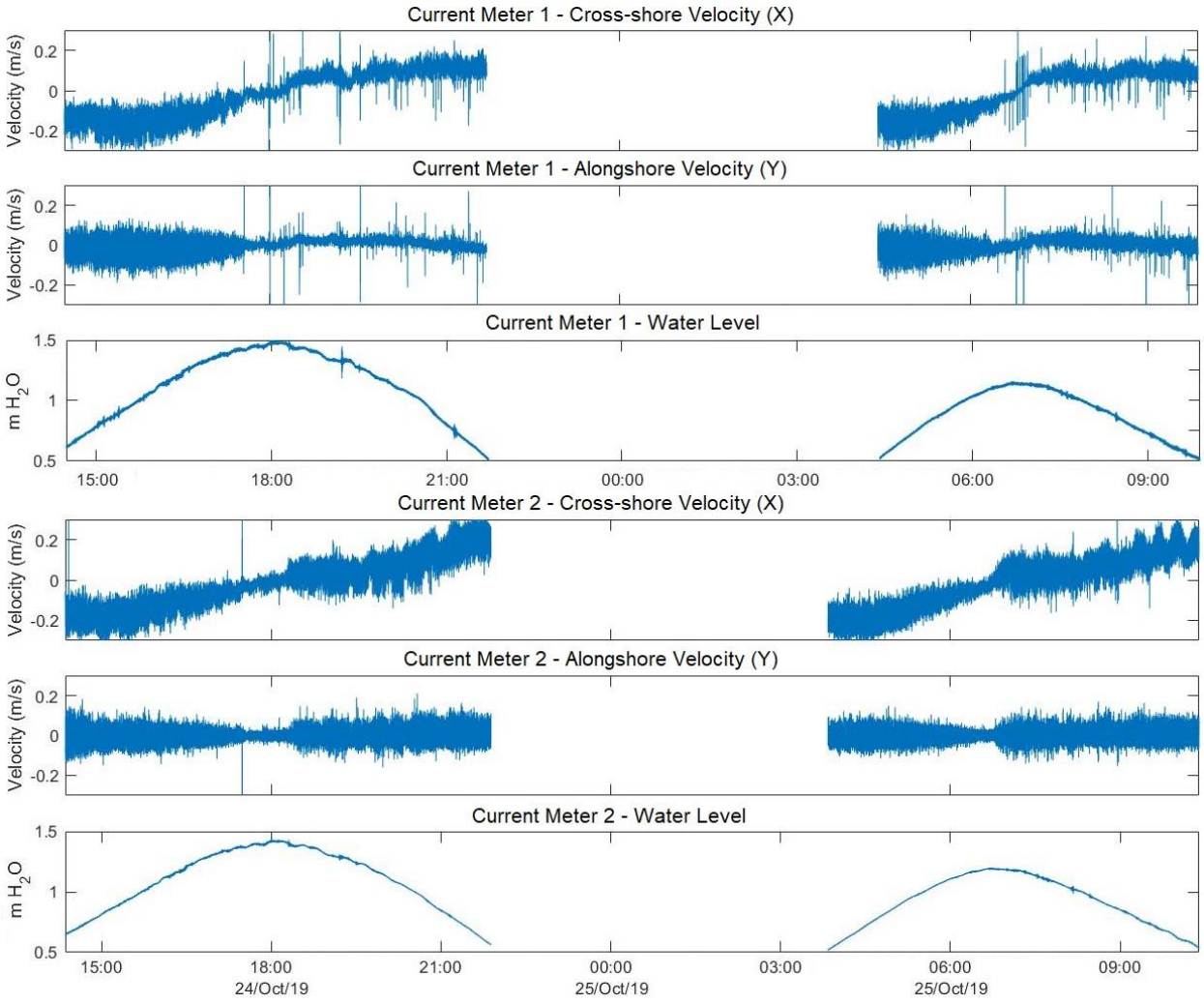

Figure 5.12. Current velocity and direction observed at opposite sides of the Port Hacking oyster reef. The X direction is cross-shore, with positive direction towards the main channel, and y direction alongshore with the positive direction towards the estuary opening (see Figure 4.3). Gaps in data are due to the devices being exposed during low tides.

5.2.5 Plaster Balls

Relative mass changes of plaster balls had a mean of 13.06%, with a standard deviation of 4.2%. Plaster ball results were mapped over the drone orthomosaic using graduated symbols and quantile classes, where size classes have an equal observation frequency (Figure 5.13). The results illustrate a concentration of the highest mass changes on the seaward side of the reef (mean of 18.3%), with particularly low changes on the inside of the reef (mean of 9.7%), as well as in seagrass regions (mean of 10.8%). The highest mass changes (21 – 22%) were recorded in the 4 plaster balls closest to the main channel. To explore any relationships between the leeward elevation shadow (identified

in Section 5.1.2) and hydraulic energy, plaster balls were separated based on the elevation contours of the sediment substrate around the reef. Using the -0.30 m contour around the reef, plaster balls inside this contour had a mean mass change (± SD) of 10.2 ± 2.2% while the points outside had a mean of 16.6 ± 3.1%. Similarly, if we use the -0.34 m contour line around the reef, we see a mean mass change of 11.1 ± 2.7% inside and 18.2 ± 2.5% outside. These results indicate that the reef creates a hydrodynamic shadow in the leeward direction of the reef, where energy within the shadow is lower than the surrounding area. The identified relationship to the elevation contours further suggests that the reefs hydrodynamic shadow is contributing to the accretion of sediment in the leeward direction.

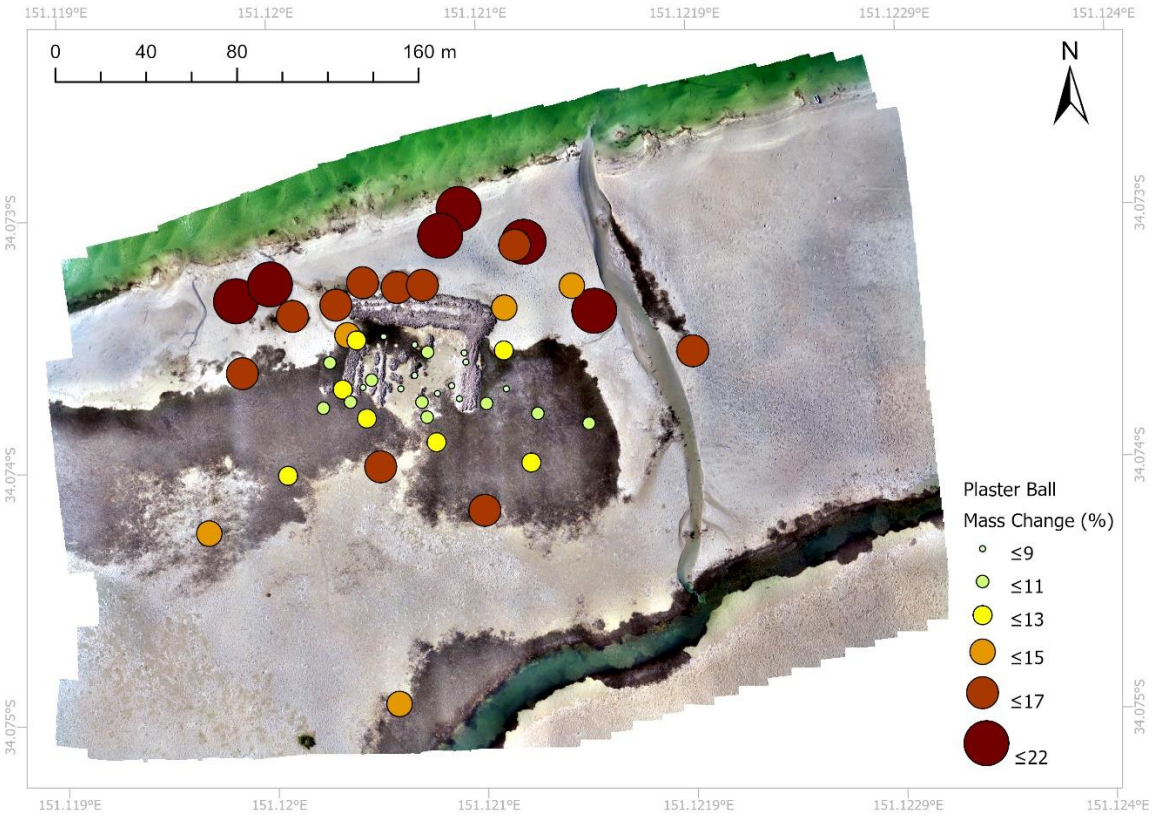

Figure 5.13. Mass change percentage of plaster balls deployed around the Port Hacking oyster reef site, overlayed on the drone orthomosaic.

5.2.6 Sediment Grainsize

Of the 60 surface sediment samples, grainsizes ranged from $3x10^{-5}$ mm to 2.1 mm, with an average of 0.25% of each sample being silt (<$3x10^{-5}$ mm) and the remainder sand ($3x10^{-5}$ mm to 2 mm) with almost no gravel identified (<0.01%). Figure 5.14 illustrates the spatial distribution of sediment samples D_{50} value (median grainsize) and sorting around the reef. A trend of poorer sorted sediment to the leeward side of the reef is apparent, indicated by larger point sizes in Figure 5.14. A similar trend in D_{50} was not so prevalent, although the poorer sorted samples were similarly found with the lowest D_{50}. No trend in the remaining values existed between seaward and leeward sides of the reef. These results illustrate that sediment textural patterns of poorly sorted sediment exist in close to the reef on the leeward side, however moving farther away from the reef we stop see any significant trends. The similar spatial trends to hydrodynamic observations with differences between seaward and leeward areas suggests that the hydrodynamic influence of the reef plays a significant role in influencing the sediment characteristics.

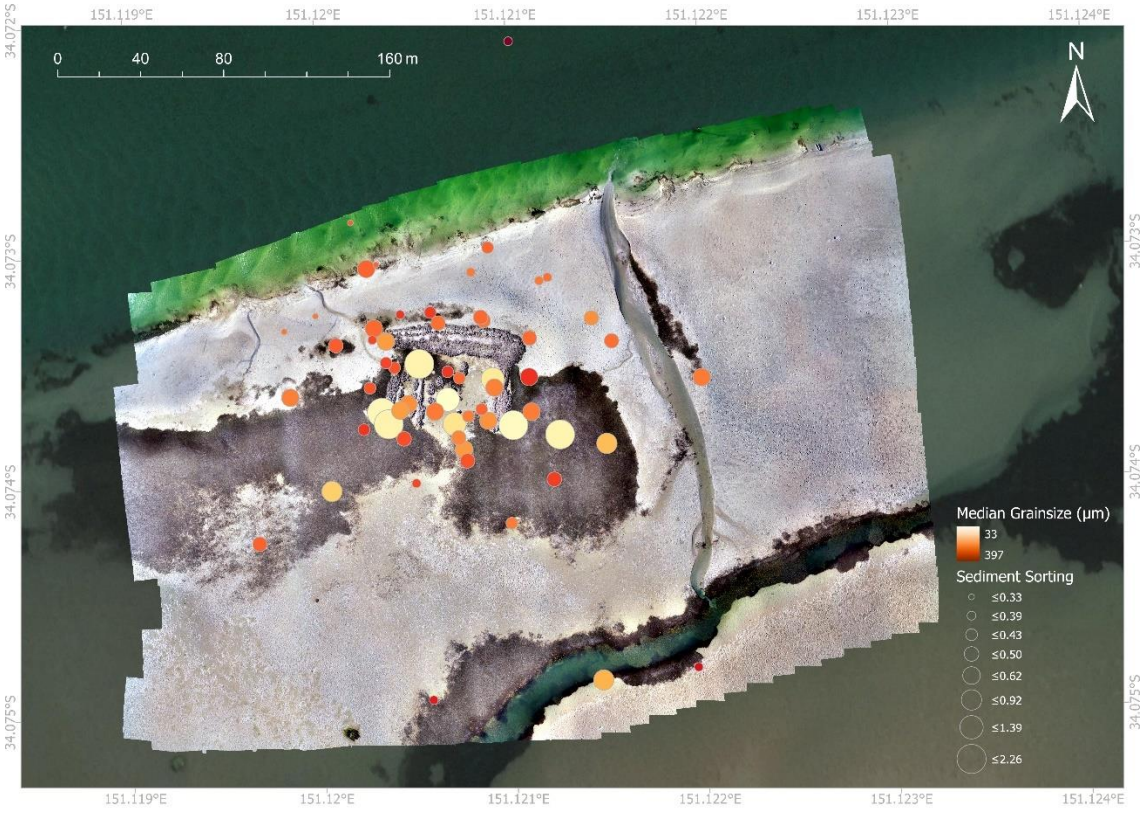

Figure 5.14. Spatial distribution of surface sediment grainsize, using sorting and median grainsize (D_{50}) measures. Sorting of samples is illustrated using the size of the point, while colour indicates the median grainsize. Poorly sorted samples are indicated by a higher uniformity value, and well sorted as a lower. Base map hybrid imagery sources: Esri, DigitalGlobe, GeoEye, i-cubed, USDA FSA, USGS, AEX, Getmapping, Aerogrid, IGN, IGP, swisstopo, and the GIS User Community.

6 Discussion

This discussion addresses the two main research aims of this project. Section 6.1 addresses the first research question: Do oyster reefs control local hydrodynamics? This section uses the environmental and topographic data of the project to identify the hydrodynamic trends and relationships around the Port Hacking oyster reef and explore their implications alongside past research. Section 6.2 addresses the second research question: Does drone data collection and processing improve the hydrodynamic study of oyster reefs? This explores the differences to past mapping techniques, including methods, processing, and outputs.

6.1 Do oyster reefs control local hydrodynamics?

The most fundamental question addressed by this thesis is whether oyster reefs influence local hydrodynamics. Past research has explored aspects of this, where Walles et al. (2015) identified an increased leeward sediment elevation likely from wave action, and Strachan (2019) and Mora (2018) also identified a leeward sediment elevation. Strachan (2019) further identified wave dissipation by a factor of 2-3 times for small wind waves (~0.5 cm). The results of this thesis build upon this by exploring additional wave attenuation characteristics (section 6.1.1), and a spatial evaluation of hydrodynamic and morphological influence from the reef (section 6.1.2).

6.1.1 Wave Attenuation

The results of wave data observed around the Port Hacking oyster reef identified two states under which significantly different wave attenuation characteristics occurred: The first was when the reef was completely submerged during high tides, and the second was when the reef was exposed during mid to low tides.

During mid to low tidal heights, when the reef was exposed by the water level, sea-swell waves were blocked by the reef and unable to penetrate the leeward areas of the

reef, observed through a significant reduction in wave height behind the reef (Figure 5.6). The second state of the reef that identified unique wave attenuation characteristics was when the reef was completely submerged. During this time sea-swell waves were able to freely pass over the reef with no significant changes in wave height, and a linear decline in height relative to the distance from the main channel. As well, an inverse interaction to infragravity waves was identified, where a linear increase in wave height was observed moving away from the main channel. Similar findings have been observed for seawalls and breakwaters, where low energy sea-well waves are able to pass over with little energy loss when tidal heights exceed the structure (Van der Meer et al., 2005). This similarity in wave attenuation characteristics to engineering structures emphasises their use as a natural engineering solution to reduce the impacts of wave action, protecting shorelines from erosion as well as sediment resuspension (Scyphers et al., 2011, Grabowski et al., 2012). Their ability to shield waves during mid to low tides can also supports adjacent ecosystems such as sea grass and mangroves, which play a further role in protecting shorelines from erosion (Spalding et al., 2014). However, the wave attenuation characteristics during high tides must also be cautioned when implementing oyster reefs where the goal is to protect shorelines or ecosystems from waves. Reef height relative to the maximum tide height will ultimately control the amount of time and sized waves that can pass over, where a taller the reef closer to the maximum tidal height will result in a smaller time window and size of waves able to pass over. This understanding will ultimately influence the size of artificial reef structures implemented in shoreline protection initiatives based on the environmental outcomes required of the restoration project. Understanding the varying wave attenuation characteristics of oyster reefs during different tidal cycles is key to building a better hydrodynamic understanding of how restoration projects will influence the environment around them, and evaluating the appropriateness of such projects.

One additional attenuation characteristic during reef exposure is wash over events from relatively high-energy waves. Indication of such events is supported by the presence of

poorly sorted sediment on the inside of the reef, where significant energy dissipation must occur to enable the larger grainsizes to be deposited with smaller grainsizes that otherwise would have been removed by such energy. This phenomenon is similarly observed in coral reef sediments, where the inner reef flats are comprised of poorly sorted sediment from high wave energy dissipation by the fringe reef (Perry et al., 2015). This is the same phenomena occurring for the Port Hacking oyster reef, where the outer reef is capable of significant energy dissipation, enabling the deposition of larger grainsizes on the inside of the reef. Sorting is further characterised in a coral reef environment by a gradient of increasing sorting as we move away from the fringe reef (Hamylton et al., 2016). Although data points past the Port Hacking reef are only few, they are increasing in sorting, suggesting a sorting gradient relative to leeward distance away from the reef may exist (Figure 5.14). Similar results were also found in adjacent seagrass to the east, which is an additional source of wave energy dissipation, as seagrass acts as a source of drag reducing current and wave energy (Luhar et al., 2017). While the number of samples were not enough to identify significance in a sorting gradient away from the reef or sea grass, this does propose a future research objective for better understanding the influence of oyster reefs on the surrounding sediment characteristics.

While the dissipation of high-energy waves causes the accumulation of poorly sorted sediments on the inside of the reef, no indication of such waves was observed in the wave spectral analysis. Sea-swell waves observed at the Port Hacking oyster reef originated from local wind sources, with winds from the north to northeast travelling over the main channel to generate waves. The narrow section of the estuary at the reef site decreases the maximum possible fetch to only a few hundred metres (Figure 3.1), minimising the potential for high energy waves to occur from wind sources. Furthermore, past research from Strachan (2019) concluded that oceanic swell was not capable of penetrating the estuary far enough to reach the reef, including during storm events. This suggests that the source of high energy waves may not be coming from

wind generated waves, but rather from artificial sources. The main channel to the north of the reef is a popular spot for recreational boat users, as well a daily ferry route linking the southern Royal National Park to the populated residential suburbs to the North. The wake from such boat traffic causes waves that travel towards the reef from north. Such waves would be larger than the wind waves observed by this project and would explain the poorly sorted sediments accumulating on the inside of the reef away from the main channel. Additionally, the wave spectral analysis performed would remove such infrequent wave events as noise. To further investigate this phenomenon, observations of boat traffic induced waves should be completed to better understand the attenuation characteristics of the reef under higher energy conditions.

6.1.2 Morphological Influence

Morphological assessment of the Port Hacking oyster reef was possible using the high-resolution drone DEM. This dataset revealed a significant sediment accretion shadow towards the southwest, many times greater than the size of the reef. Hydrodynamic forcing's that influence this include the observed tidal currents and wave energy, as well as the inferred higher energy waves from boat traffic. While it is difficult to distinguish the influence of each hydrodynamic forcing on shaping the sediment shadow, each agrees with the morphological development in the south to southwest direction through a reduction in hydrodynamic energy on the leeward side of the reef. Additionally, the results comparing the prior RTK-GNSS and more recent drone DEM suggest that the sediment shadow is continuing to accrete over time. These observations are all in line with conclusions from Walles et al. (2015) that sediments will accumulate on the leeward side of the reef from the direction of hydrodynamic energy.

Understanding the scale of morphological influence oyster reefs have in the surrounding environment is key when assessing their application in restoration projects. Instances where reefs are used as an ecological engineering solution for shoreline protection, the

placement of the reef must consider the scale of influence the reef has on controlling sediment accretion and erosion. Past projects have implemented reefs within metres of the shoreline to protect from erosion or wave action to sensitive ecosystems such as salt marshes (Scyphers et al., 2011). The extended area of influence identified by this project means that a similar protection and sediment accretion could still be attained by placing reefs further from the shoreline, maximising the area protected by restoration reefs. This aspect requires further attention, investigating how the size and distance of restoration reefs from shorelines can effectively maintain the various goals of shoreline protection.

6.2 Does drone data collection and processing benefit the hydrodynamic study of oyster reefs?

The second question within the aims of this thesis is whether drone data collection and processing benefit the hydrodynamic study of oyster reefs. This discussion is organised into subsections, each of which represents a significant change in incorporating drone data collection and processing to the study of oyster reefs and hydrodynamics. Section 6.3.1 addresses the accuracy and resolution of drone data collection with traditional methods. Section 6.3.2 explores the role of drones in improving the physical access issues to oyster reefs. And section 6.3.3 addresses the complications of photogrammetric data processing through specific software packages.

6.2.1 Accuracy and Resolution

The photogrammetric processing of drone data and GCPs resulted in a DEM of the Port Hacking oyster reef with a total error of 3.64 cm, including errors of 0.72 cm, 0.71 cm, and 3.50 cm in the X/Y/Z domains, respectively. Although these results are aligned with research by Martínez-Carricondo et al. (2018) that horizontal accuracy (X/Y) will be higher than the vertical (Z), our results indicate a much greater discrepancy between the two. This discrepancy is particularly noticeable around the highest elevation points of

the oyster reef (Table 5.1), suggesting that the complex 3-dimensional reef structures present complications for photogrammetric algorithms, and that the overall accuracy of the model outside the reef area is higher than then the calculated RMSE. The high errors on the reef may also be in part due to the resolution of the survey. The results of our survey computed a resolution of 2.86 cm per pixel. With the mean maximum oyster length of the *Saccostrea glomerata* (Sydney rock oyster) for the east coast of Australia estimated to be 3.57 cm (McLeod et al., 2019), we can assume that the resolution of our survey is not capable of modelling the structure of the reef to an individual oyster level. For this reason, a smoothing effect would occur over the reef where gaps between or extruding oysters are smoothed over. The impact of this would cause variations between the DEM model and the actual reef structure and would explain the higher errors observed over the more complex and varying 3-dimensional reef structure. This effect could be minimised by performing a higher resolution drone survey, completed by flying the drone at a lower altitude over the reef and with a tighter grid pattern to maintain image overlap parameters. For example, to double the image resolution of the drone survey, a flight altitude of 14m or lower would have to be achieved, resulting in a minimum 195 min drone flight over the 373 x 290 m area. Future flight plans should consider the associated errors of different survey parameters, ensuring errors are acceptable for the analysis intended.

In comparison to past research, we can observe the differences in resolution to understand the benefits of drone technology as a survey technique for Oyster reef hydrodynamics. The surface model of individual oyster reefs performed by Walles et al. (2015) achieved a model resolution of 2 - 4 m using RTK-GNSS point sampling and linear interpolation. The model by Strachan (2019) used a similar method of RTK-GNSS point sampling and interpolation to develop a model of the Port Hacking oyster reef with an interpolated resolution of 1 m, with a point density of 1 point per 23.7 m^2. Similarly, the RTK-GNSS model from this project resulted in 0.98 m resolution DEM, with a data point density of 1 point per 11.2 m^2. Complications in the RTK-GNSS

methodology stem from a sparse and irregular data coverage which results in large errors from the interpolation process (Drummond et al., 2015). This creates difficulty in statistically comparing the accuracy results with drone models, as reliability and errors vary spatially across the model. However, the comparison of data point density gives an insight into the possible resolution outputs between with the different techniques. The data point density of this projects RTK-GNSS survey resulted 0.09 m^2, compared to the drones 2039.1 points per m^2, based on the image tie points, resulting in a data point density increase of 22,838 times. It must be noted that the number of tie points may be slightly lower as errors occur in the structure from motion processing resulting in some tie points misaligned E.g. reflection or distortion from water surfaces. We can also visually observe the comparisons in Figure 6.1 to identify the drastic increase in the detail between the two methods. The resolution of the drone model allows for identification of additional features such as drainage patterns throughout the sediment substrate, seagrass vegetation, distinct channel boundaries, and sediment morphology. Another significant benefit of the drone survey is the ability to generate an orthomosaic (Figure 5.2). This visualisation of the survey area aids in the analysis of topographic features, as well as the ability to identify features and spatial patterns not possible from the ground. Increasing both the resolution and accuracy of a survey, regardless of the subject, enables a more in-depth and precise understanding of the underlying processes.

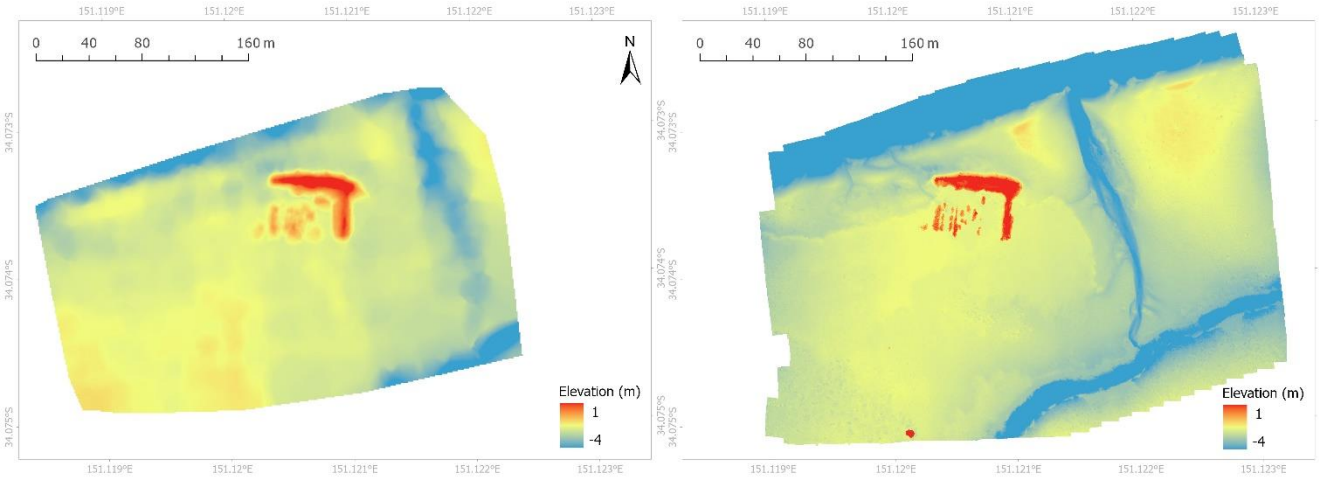

Figure 6.1. Comparison between the digital elevation models from the RTK-GNSS survey (left) with the drone survey (right) for the Port Hacking oyster reef.

When establishing the errors associated with a model, we must also consider the human errors associated with data collection. Since the drone data collection is an automated process, the human error is associated with the collection of GCPs. The RTK-GNSS receiver, mounted to a 2 m carbon pole, must be manually held in place while the positional data is recorded. Errors in this collection arise as the device under its own weight would penetrate the sediment surface, and so the user suspends the device as close as possible to the surface. This adds potential for errors as the device may be held slightly above or below the actual surface height. Although this error is difficult to quantify, we must acknowledge that the 15 mm vertical accuracy of the device is further complicated by human errors. Potential to remove this human error includes the use of a tripod to vertically align and lower the RTK-GNSS to the exact height of the surface. This may be considered by future studies, which may require higher accuracy.

6.2.2 Access

One of the main issues with the study of oyster reefs is that they are often located in tidal zones that are completely submerged during the high tide. This means that access is only possible for a limited time during low tides, often only by boat, and subject to weather conditions. This is the case for the Port Hacking oyster reef (Figure 3.1) where boat access is required, and access is limited to low tide. Area around the reef also contains sensitive regions of sea grass, also considered an important ecosystem engineer that creates, develops, and maintains habitat for other species (Walles et al., 2015, de Paiva et al., 2018). Performing an RTK-GNSS survey of the Port Hacking oyster reef and surrounding sediment substrate involves walking over and through the reef and sea grass beds. This is a destructive practice that comes at an environmental cost to its completion. Although drone survey techniques involve the collection of GCP points similarly using an RTK-GNSS, markers can be strategically placed to ensure collection

does not involve any destruction to the existing environment. This methodology for data collection ensures a minimal environmental impact that can be tailored to suit different survey areas.

When looking to perform multiple surveys, drones have the potential to further lower the costs associated. GCP markers for a survey can include physical features identifiable in aerial imagery instead of placed markers (Westoby et al., 2012). If these are permanent features, collecting the coordinates once is sufficient to perform multiple surveys and continue using the same markers in future surveys. Permanent markers can also be deployed, for example such as sand stakes around an oyster reef. Once markers have been identified, drone surveys do not have the requirement to be performed from the site, rather they can be performed from a nearby shoreline where access is possible by car or foot. For example, the drone for this project was a DJI Phantom Pro 4 capable of a maximum flight range of 7 km from the controller (LCC, 2019). This enables the survey to theoretically be performed from anywhere within a 7 km radius of the study site if permanent markers are identified. Without the need to be on the reef site, survey costs are reduced as a boat is not required, and there is no environmental impact to the reef for further surveys. Human effort is also minimal due to the automated drone flight, and the time required is drastically reduced compared to traditional RTK-GNSS surveys. These access benefits of drone survey techniques provide users with the ability to perform higher frequency surveys with reduced human effort, and at a minimised environmental impact.

Although many benefits of drone survey techniques exist, there are still limitations that affect their access. The ability to operate a drone is subject to the local flight restrictions, such as no fly zones or restricted altitudes. Examples include nearby airports enforcing no-fly zones, national parks restricting flights to permit holders, or protected areas banning flights due to potential negative impacts to local species. For the Port Hacking oyster reef, limitations included a flight altitude limit of 120 m, a 30 m

minimum distance from any person (besides the controller), and the drone cannot be flown directly above people regardless of distance. Although these restrictions did not affect the possibility to survey the Port Hacking reef, they must be considered for any survey to evaluate the access limitations of drone data collection. Furthermore, drone licences may be required in certain regions, and depending on the intention of the flight for research or commercial purposes. To confirm such requirements, local aviation authorities should be contacted, and the relevant permits and licences obtained.

6.2.3 Software

The photogrammetric software, Agisoft Metashape Professional, used for this project has been identified as the most accurate software for SFM photogrammetric techniques (Martínez-Carricondo et al., 2018). However, there are high amounts of input parameters and processing variables that influences a user's ability to produce accurate results. As outlined in Chapter 4.4 and Appendix 9.1, there are several different steps, each with many parameters to be determined to obtain a final DEM. The choice of these parameters influences the accuracy of the results, and currently has been no research into optimising parameters based on survey specifications. Additionally, parameter selection is dependent on the processing power of the computer and time available. The errors identified in our model may not be the lowest possible but were the best result obtained with the computer processing power and time available. This point is important to consider when assessing the application of drone technology to future studies and requires further research attention to enable more users.

6.3 Implications of Results

Despite the initiation of Australian oyster reef restoration projects, and a subsequent growth in attention, there is still a lack of understanding surrounding their impacts (Gillies et al., 2018). This is an ongoing process for research, building upon past efforts and continuing to further the understanding. The results of this thesis add spatial trends

of sedimentation to provide insight into the scale of hydrodynamic influence from oyster reefs, as well as the mechanisms involved. While there is still a long way to go in developing an understanding of reef restoration, this project is an important step in incorporating new technology to further this research.

In the face of climate change, one of the important benefits of oyster reef hydrodynamics is their potential as natural engineering structures (Spalding et al., 2014, Scyphers et al., 2011). Shoreline erosion has increasingly become of concern within estuarine environments (de Paiva et al., 2018, Scyphers et al., 2011), where sea-level rise threatens both ecosystems and infrastructure. The hydrodynamic influence of oyster reefs identified by this research confirms their potential as a viable solution to increase sediment accretion on the leeward side, while stabilising the sediment underfoot to prevent erosion. The use of oyster reefs as a natural engineering solution over traditional methods, such as breakwaters, is that they develop an ecosystem. Oyster reefs create, develop, and maintain habitat for a variety of species within the estuarine environment, creating an ecosystem that benefits the health and productivity of the estuary (Scyphers et al., 2011). This technique of natural engineering also has the capabilities to modify and adapt to climate change with time. Past research has illustrated this through oyster reefs growth rate being able to keep pace with sea-level rise (Rodriguez et al., 2014). Unlike man-made engineering structures that must be modified or replaced to suit, oyster reefs may ensure a sustained protection into the future. An additional benefit of oyster reefs over man-made structures is their ecosystem services, as they facilitate more diverse fish and invertebrate species through habitat enhancement (Scyphers et al., 2011). While these benefits of oyster reefs as a natural engineering solution highlight their potential as an adaptive and positive ecosystem solution in the face of climate change, there must still be caution taken when initiating such projects. The scale of hydrodynamic influence identified in this project causes a sediment accretion shadow many times the size of the reef. Understanding of how this influences estuarine sediment transport on a system wide scale is still

unknown. Many ecosystems have developed around the natural sediment transportation regime of estuaries and impacts of modifying this may be detrimental. Until the impacts of restoration are understood on a system wide scale, caution must be taken when selecting the application of oyster reef restoration.

6.4 Future Research

To further the hydrodynamic study of oyster reefs, higher-energy waves should be investigated to better understand the attenuation capabilities of reef structures. Sediment results from this thesis identified evidence of higher-energy waves being dissipated by the reef but did not observe examples of this in wave data. Furthering this understanding of oyster reef attenuation capabilities is key in better anticipating the implications of restoration projects and how different wave characteristics influence the surrounding sediment morphology.

The proposed data collection methods using drones presents benefits for biological research in tracking reef growth. High-resolution 3-dimensional models enable comprehensive growth patterns to be identified on oyster reefs overtime. Past RTK-GNSS techniques are difficult to complete for high resolution 3-dimensional structures, impossible for larger reefs, and can be destructive to the reef when taking measurements. The non-invasive nature and high resolution of drone data collection provides a perfect platform to monitor and identify physical changes in the reef. Performed in collaboration with a hydrodynamic analysis, this research could better understand the relationships between sediment food delivery mechanisms and growth patterns.

7 Conclusion

With this thesis, we conclude that oyster reefs do play a significant role in controlling the local hydrodynamics of estuarine environments, and that drones significantly improve the hydrodynamic study of oyster reefs. These answers to the research aims were reached based on the following conclusions and that build upon the findings of past research:

(1) A hydrodynamic shadow exists on the leeward side of the reef, significantly greater than the reef size (Figure 7.1).

Morphological assessment of the sediment substrate surrounding an oyster reef revealed a hydrodynamic shadow, significantly greater than the size of the reef, accumulating sediment within. Direction of the shadow is categorised by the direction of flood tide currents, and wind generated waves.

(2) Oyster reefs act as a physical barrier to small wind wave energy, until the tide height exceeds the reef height and waves can pass over with minimal obstruction.

Hydrodynamic protection from wind generated waves (0.2 – 1.9 cm) occurs on the leeward side of the reef while the reef is exposed by the water level. Once the reef is submerged, waves can pass over the reef with minimum interference.

(3) Textural patterns in sediment surrounding oyster reefs suggest that higher-energy waves are dissipated by oyster reefs.

Poorly sorted sediments on the inner reef indicate higher wave energy dissipation by the reef, enabling the accumulation of larger sediment grainsizes in a predominantly fine sand environment.

(4) Drone data collection provides high resolution and accurate elevation modelling of oyster reefs and the surrounding sediment substrate, drastically improving the results of past techniques.

The application of drone technology to the study of oyster reefs provides a new spatial data collection technique, significantly advancing the results to enable more detailed and precise analysis. This technique also minimises the environmental impact during data collection while reducing the human effort required.

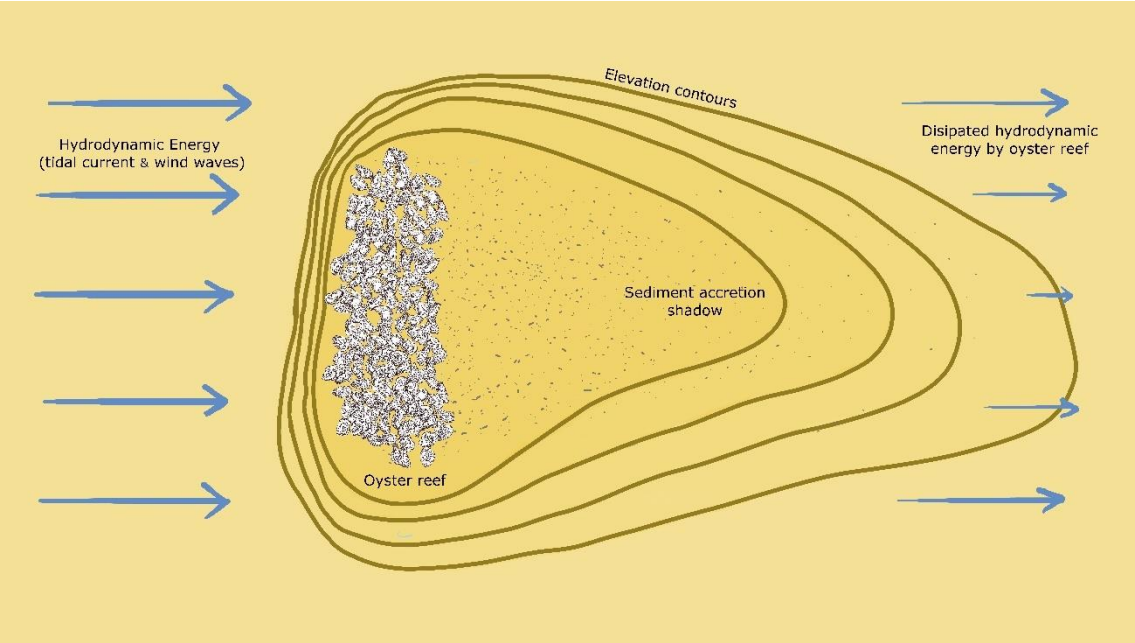

Figure 7.1. Conceptual model of the sediment accretion shadow that occurs in the leeward direction of the reef. The shadow extends many times the size of the reef, with increased elevation in close to the reef. Poorly sorted sediment occurs on the leeward side, with sorting increasing moving away from the reef. Hydrodynamic energy dissipation over the reef enables the accumulation of sediment, ultimately controlling the direction and extent of the shadow.

8 References

ADAMS, J., PRETORIUS, L. & SNOW, G. 2019. Deterioration in the water quality of an urbanised estuary with recommendations for improvement. *Water SA,* 45**,** 86-96.

ALBANI, A. & COTIS, G. 2007. Port Hacking: Past and Present. *New South Wales Department of Environment and Climate Change, Sydney*.

ALLEWAY, H., COOK, P., CRAWFORD, C., CREIGHTON, C., DIGGLES, B., FORD, J., GILLIES, C., HAMER, P., LEBRAULT, E. & LE PORT, A. 2015. Shellfish reef habitats: a synopsis to underpin the repair and conservation of Australia's environmental, social and economically important bays and estuaries.

ALLEWAY, H. K. & CONNELL, S. D. 2015. Loss of an ecological baseline through the eradication of oyster reefs from coastal ecosystems and human memory. *Conservation Biology,* 29**,** 795-804.

BARBIER, E. B., HACKER, S. D., KENNEDY, C., KOCH, E. W., STIER, A. C. & SILLIMAN, B. R. 2011. The value of estuarine and coastal ecosystem services. *Ecological monographs,* 81**,** 169-193.

BIRCH, G. 2006. A short geological and environmental history. Sydney University Press.

BODANSKY, E., GRIBOV, A. & PILOUK, M. Smoothing and compression of lines obtained by raster-to-vector conversion. International Workshop on Graphics Recognition, 2001. Springer, 256-265.

BRUCE, E. M. & ELIOT, I. G. 2006. A spatial model for marine park zoning. *Coastal Management,* 34**,** 17-38.

CAMPBELL, M. D. & HALL, S. G. 2019. Hydrodynamic effects on oyster aquaculture systems: a review. *Reviews in Aquaculture,* 11**,** 896-906.

CATON, B. & HARVEY, N. 2010. *Coastal management in Australia*, University of Adelaide Press.

CHRISTIE, P. 2005. Is integrated coastal management sustainable? *Ocean & Coastal Management,* 48**,** 208-232.

COLOMINA, I. & MOLINA, P. 2014. Unmanned aerial systems for photogrammetry and remote sensing: A review. *ISPRS Journal of photogrammetry and remote sensing,* 92**,** 79-97.

DALAMAGKIDIS, K., VALAVANIS, K. P. & PIEGL, L. A. 2012. Aviation history and unmanned flight. *On integrating unmanned aircraft systems into the national airspace system.* Springer.

DAY JR, J. W., KEMP, W. M., YÁÑEZ-ARANCIBIA, A. & CRUMP, B. C. 2012. *Estuarine ecology*, John Wiley & Sons.

DE PAIVA, J. N. S., WALLES, B., YSEBAERT, T. & BOUMA, T. J. 2018. Understanding the conditionality of ecosystem services: The effect of tidal flat morphology and oyster reef characteristics on sediment stabilization by oyster reefs. *Ecological Engineering,* 112**,** 89-95.

DRUMMOND, C. D., HARLEY, M. D., TURNER, I. L., A MATHEEN, A. N. & GLAMORE, W. C. UAV applications to coastal engineering. Australasian Coasts & Ports Conference 2015: 22nd Australasian Coastal and Ocean Engineering Conference and the 15th Australasian Port and Harbour Conference, 2015. Engineers Australia and IPENZ, 267.

EPA, N. 1997. Protection of the Environment Operations Act 1997. *NSW Consolidated Act. (http://www.austlii.edu.au/au/legis/nsw/consol_act/poteoa1997455/).*

FANG, Q., MA, D., ZHANG, L. & ZHU, S. 2018. Marine functional zoning: A practical approach for integrated coastal management (ICM) in Xiamen. *Ocean & Coastal Management***,** 104433.
GARDNER, R. C. & DAVIDSON, N. C. 2011. The ramsar convention. *Wetlands.* Springer.
GERTLER, J. US unmanned aerial systems. 2012. Library of Congress Washington DC Congressional Research Service.
GILLIES, C. L., MCLEOD, I. M., ALLEWAY, H. K., COOK, P., CRAWFORD, C., CREIGHTON, C., DIGGLES, B., FORD, J., HAMER, P. & HELLER-WAGNER, G. 2018. Australian shellfish ecosystems: Past distribution, current status and future direction. *PloS one,* 13.
GOLLIN, D., JEDWAB, R. & VOLLRATH, D. 2016. Urbanization with and without industrialization. *Journal of Economic Growth,* 21**,** 35-70.
GONÇALVES, J. & HENRIQUES, R. 2015. UAV photogrammetry for topographic monitoring of coastal areas. *ISPRS Journal of Photogrammetry and Remote Sensing,* 104**,** 101-111.
GRABOWSKI, J. H., BRUMBAUGH, R. D., CONRAD, R. F., KEELER, A. G., OPALUCH, J. J., PETERSON, C. H., PIEHLER, M. F., POWERS, S. P. & SMYTH, A. R. 2012. Economic valuation of ecosystem services provided by oyster reefs. *Bioscience,* 62**,** 900-909.
GRABOWSKI, J. H. & PETERSON, C. H. 2007. Restoring oyster reefs to recover ecosystem services. *Ecosystem engineers: plants to protists,* 4**,** 281-298.
GUPTA, L., JAIN, R. & VASZKUN, G. 2015. Survey of important issues in UAV communication networks. *IEEE Communications Surveys & Tutorials,* 18**,** 1123-1152.
HAMYLTON, S. M., CARVALHO, R. C., DUCE, S., ROELFSEMA, C. M. & VILA-CONCEJO, A. 2016. Linking pattern to process in reef sediment dynamics at Lady Musgrave Island, southern Great Barrier Reef. *Sedimentology,* 63**,** 1634-1650.
HARRIS, P., MUELBERT, J., MUNIZ, P., YIN, K., AHMED, K., FOLORUNSHO, R., CASO, M., VALE, C. C., MACHIWA, J. & FERREIRA, B. 2016a. Estuaries and Deltas.
HARRIS, P., MUELBERT, J., MUNIZ, P., YIN, K., AHMED, K., FOLORUNSHO, R., CASO, M., VALE, C. C., MACHIWA, J. & FERREIRA, B. 2016b. . Estuaries and Deltas.
HART, J. K. & MARTINEZ, K. 2006. Environmental sensor networks: A revolution in the earth system science? *Earth-Science Reviews,* 78**,** 177-191.
HOFFMANN, R. C. 2005. A brief history of aquatic resource use in medieval Europe. *Helgoland Marine Research,* 59**,** 22-30.
JIANG, A. W., RANASINGHE, R. & COWELL, P. 2013. Contemporary hydrodynamics and morphological change of a microtidal estuary: a numerical modelling study. *Ocean Dynamics,* 63**,** 21-41.
JONES, C. G., LAWTON, J. H. & SHACHAK, M. 1994. Organisms as ecosystem engineers. *Ecosystem management.* Springer.
JOYCE, K., DUCE, S., LEAHY, S., LEON, J. & MAIER, S. 2019. Principles and practice of acquiring drone-based image data in marine environments. *Marine and Freshwater Research,* 70**,** 952-963.
KENCH, P. S. 1999. Geomorphology of Australian estuaries: review and prospect. *Australian Journal of Ecology,* 24**,** 367-380.

KJERFVE, B. 2018. *Hydrodynamics of Estuaries: Volume I Estuarine Physics*, CRC Press.
KLEMAS, V. V. 2015. Coastal and environmental remote sensing from unmanned aerial vehicles: An overview. *Journal of coastal research,* 31**,** 1260-1267.
KOVALIC, J. M. 1987. Clean Water Act of 1987. The Water Environment Federation.
KULMAR, M., MODRA, B. & FITZHENRY, M. The New South Wales wave climate improved understanding through the introduction of directional wave monitoring buoys. Coasts and Ports 2013: 21st Australasian Coastal and Ocean Engineering Conference and the 14th Australasian Port and Harbour Conference, 2013. Engineers Australia, 453.
LANGHAMMER, J., BERNSTEINOVÁ, J. & MIŘIJOVSKÝ, J. 2017. Building a high-precision 2D hydrodynamic flood model using UAV photogrammetry and sensor network monitoring. *Water,* 9**,** 861.
LCC, A. 2019. Agisoft Metashape User Manual: Professional Edition, Version 1.5. *St. Petersburg, Russia*.
LEVASSEUR, A., SHI, L., WELLS, N. C., PURDIE, D. A. & KELLY-GERREYN, B. A. 2007. A three-dimensional hydrodynamic model of estuarine circulation with an application to Southampton Water, UK. *Estuarine, Coastal and Shelf Science,* 73**,** 753-767.
LINDER, W. 2009. *Digital photogrammetry*, Springer.
LOTZE, H. K., LENIHAN, H. S., BOURQUE, B. J., BRADBURY, R. H., COOKE, R. G., KAY, M. C., KIDWELL, S. M., KIRBY, M. X., PETERSON, C. H. & JACKSON, J. B. 2006. Depletion, degradation, and recovery potential of estuaries and coastal seas. *Science,* 312**,** 1806-1809.
LUHAR, M., INFANTES, E. & NEPF, H. 2017. Seagrass blade motion under waves and its impact on wave decay. *Journal of Geophysical Research: Oceans*, 122**,** 3736-3752.
LUNT, J., REUSTLE, J. & SMEE, D. L. 2017. Wave energy and flow reduce the abundance and size of benthic species on oyster reefs. *Marine Ecology Progress Series,* 569**,** 25-36.
MANCINI, F., DUBBINI, M., GATTELLI, M., STECCHI, F., FABBRI, S. & GABBIANELLI, G. 2013. Using unmanned aerial vehicles (UAV) for high-resolution reconstruction of topography: The structure from motion approach on coastal environments. *Remote sensing*, 5**,** 6880-6898.
MARTÍNEZ-CARRICONDO, P., AGÜERA-VEGA, F., CARVAJAL-RAMÍREZ, F., MESAS-CARRASCOSA, F.-J., GARCÍA-FERRER, A. & PÉREZ-PORRAS, F.-J. 2018. Assessment of UAV-photogrammetric mapping accuracy based on variation of ground control points. *International journal of applied earth observation and geoinformation,* 72**,** 1-10.
MAYER-PINTO, M., JOHNSTON, E., HUTCHINGS, P., MARZINELLI, E., AHYONG, S., BIRCH, G., BOOTH, D., CREESE, R., DOBLIN, M. & FIGUEIRA, W. 2015. Sydney Harbour: a review of anthropogenic impacts on the biodiversity and ecosystem function of one of the world's largest natural harbours. *Marine and Freshwater Research,* 66**,** 1088-1105.
MCLEOD, I., BOSTRÖM-EINARSSON, L., CREIGHTON, C., D'ANASTASI, B., DIGGLES, B., DWYER, P., FIRBY, L., LE PORT, A., LUONGO, A. & MARTÍNEZ-BAENA, F. 2019. Habitat value of Sydney rock oyster (Saccostrea glomerata) reefs on soft sediments. *Marine and Freshwater Research*.
MCLUSKY, D. S. & ELLIOTT, M. 2004. *The estuarine ecosystem: ecology, threats and management*, OUP Oxford.

MEIRE, P., YSEBAERT, T., VAN DAMME, S., VAN DEN BERGH, E., MARIS, T. & STRUYF, E. 2005. The Scheldt estuary: a description of a changing ecosystem. *Hydrobiologia,* 540**,** 1-11.

MLAMBO, R., WOODHOUSE, I. H., GERARD, F. & ANDERSON, K. 2017. Structure from motion (SfM) photogrammetry with drone data: A low cost method for monitoring greenhouse gas emissions from forests in developing countries. *Forests,* 8**,** 68.

MORA, C. 2018. *The effects of oyster reefs on local hydrodynamics and metal-contaminated sediments.* BSc (Hons), The University of Sydney.

NAUGHTON, R. 2007. Remote piloted aerial vehicles: An anthology. *Centre for Telecommunications and Information Engineering, Monash University,* 3.

NEX, F. & REMONDINO, F. 2014. UAV for 3D mapping applications: a review. *Applied geomatics,* 6**,** 1-15.

O'NEIL, J. M., TAILLIE, D., WALSH, B., DENNISON, W. C., BONE, E. K., REID, D. J., NEWTON, R., STRAYER, D. L., BOICOURT, K. & BIRNEY, L. B. 2016. New York Harbor: Resilience in the face of four centuries of development. *Regional studies in marine science,* 8**,** 274-286.

PENDLETON, L. 2009. The economic and market value of America's coasts and estuaries: what's at stake. *Coastal Ocean Values Press, Washington, DC*.

PERRY, C. T., KENCH, P. S., O'LEARY, M., MORGAN, K. & JANUCHOWSKI-HARTLEY, F. 2015. Linking reef ecology to island building: Parrotfish identified as major producers of island-building sediment in the Maldives. *Geology,* 43**,** 503-506.

POTTER, I. C., CHUWEN, B. M., HOEKSEMA, S. D. & ELLIOTT, M. 2010. The concept of an estuary: a definition that incorporates systems which can become closed to the ocean and hypersaline. *Estuarine, Coastal and Shelf Science,* 87**,** 497-500.

REIDENBACH, M. A., BERG, P., HUME, A., HANSEN, J. C. & WHITMAN, E. R. 2013. Hydrodynamics of intertidal oyster reefs: The influence of boundary layer flow processes on sediment and oxygen exchange. *Limnology and Oceanography: Fluids and Environments,* 3**,** 225-239.

RIDGE, J. T., RODRIGUEZ, A. B. & FODRIE, F. J. 2017. Evidence of exceptional oyster-reef resilience to fluctuations in sea level. *Ecology and evolution,* 7**,** 10409-10420.

RODRIGUEZ, A. B., FODRIE, F. J., RIDGE, J. T., LINDQUIST, N. L., THEUERKAUF, E. J., COLEMAN, S. E., GRABOWSKI, J. H., BRODEUR, M. C., GITTMAN, R. K. & KELLER, D. A. 2014. Oyster reefs can outpace sea-level rise. *Nature climate change,* 4**,** 493-497.

ROY, P., WILLIAMS, R., JONES, A., YASSINI, I., GIBBS, P., COATES, B., WEST, R., SCANES, P., HUDSON, J. & NICHOL, S. 2001. Structure and function of south-east Australian estuaries. *Estuarine, Coastal and Shelf Science,* 53**,** 351-384.

ROY, P. S. 1994. Holocene estuary evolution—stratigraphic studies from southeastern Australia.

SCYPHERS, S. B., POWERS, S. P., HECK JR, K. L. & BYRON, D. 2011. Oyster reefs as natural breakwaters mitigate shoreline loss and facilitate fisheries. *PloS one,* 6.

SEYMOUR, A., RIDGE, J., RODRIGUEZ, A., NEWTON, E., DALE, J. & JOHNSTON, D. 2018. Deploying fixed wing Unoccupied Aerial Systems

(UAS) for coastal morphology assessment and management. *Journal of Coastal Research,* 34**,** 704-717.
SIMCOCK, A., HALPERN, B., KIRUBAGARAN, R., HOSSEIN, M., POLETTE, M., SMITH, E. & INNISS, L. 2016. Coastal, riverine and atmospheric inputs from land. *Inniss L, Simcock A, coordinators. First Global Integrated Marine Assessment. United Nations***,** 1-93.
SMITH, T. F., SANT, M. & THOM, B. 2001. Australian Estuaries: A framework for management. *Australian estuaries: a framework for management*.
SPALDING, M. D., RUFFO, S., LACAMBRA, C., MELIANE, I., HALE, L. Z., SHEPARD, C. C. & BECK, M. W. 2014. The role of ecosystems in coastal protection: Adapting to climate change and coastal hazards. *Ocean & Coastal Management,* 90**,** 50-57.
STRACHAN, I. 2019. *Ecosystem services of oyster reefs in microtidal estuaries: biodeposition of trace metals and wave attenuation.* BSc (Hons), The University of Sydney.
VAN DER MEER, J. W., BRIGANTI, R., ZANUTTIGH, B. & WANG, B. 2005. Wave transmission and reflection at low-crested structures: Design formulae, oblique wave attack and spectral change. *Coastal Engineering,* 52**,** 915-929.
VAN NIEKERK, L., ADAMS, J., BATE, G., FORBES, A., FORBES, N., HUIZINGA, P., LAMBERTH, S., MACKAY, C., PETERSEN, C. & TALJAARD, S. 2013. Country-wide assessment of estuary health: An approach for integrating pressures and ecosystem response in a data limited environment. *Estuarine, coastal and shelf science,* 130**,** 239-251.
VERMAAT, J. E., AGAWIN, N., FORTES, M., URI, J., DUARTE, C., MARBA, N., ENRIQUEZ, S. & VAN VIERSSEN, W. 1997. The capacity of seagrasses to survive increased turbidity and siltation: the significance of growth form and light use. *Ambio,* 26**,** 499-504.
VILES, H. & SPENCER, T. 2014. *Coastal problems: geomorphology, ecology and society at the coast*, Routledge.
WALLES, B., DE PAIVA, J. S., VAN PROOIJEN, B. C., YSEBAERT, T. & SMAAL, A. C. 2015. The ecosystem engineer Crassostrea gigas affects tidal flat morphology beyond the boundary of their reef structures. *Estuaries and coasts,* 38**,** 941-950.
WESTOBY, M. J., BRASINGTON, J., GLASSER, N. F., HAMBREY, M. J. & REYNOLDS, J. M. 2012. 'Structure-from-Motion'photogrammetry: A low-cost, effective tool for geoscience applications. *Geomorphology,* 179**,** 300-314.
WOLANSKI, E. & ELLIOTT, M. 2015. *Estuarine ecohydrology: an introduction*, Elsevier.
YOKOYAMA, H., INOUE, M. & ABO, K. 2004. Estimation of the assimilative capacity of fish-farm environments based on the current velocity measured by plaster balls. *Aquaculture,* 240**,** 233-247.
ZALOGA, S. J. 2011. *Unmanned aerial vehicles: robotic air warfare 1917–2007*, Bloomsbury Publishing.

9 Appendix

9.1 Photogrammetric Software Processing Parameters

General	
Cameras	1292
Aligned cameras	1292
Markers	21
Coordinate system	GDA94/MGA zone 56 (EPSG::28356)
Rotation angles	Yaw, Pitch, Roll
Point Cloud	
Points	2,378,261 of 2,823,271
RMS reprojection error	0.114825 (0.949687 pix)
Max reprojection error	0.475096 (45.9987 pix)
Mean key point size	6.93776 pix
Point colours	3 bands, uint8
Key points	No
Average tie point multiplicity	5.51898
Alignment parameters	
Accuracy	Medium
Generic preselection	No
Reference preselection	Source
Key point limit	80,000
Tie point limit	No
Guided image matching	No
Adaptive camera model fitting	Yes
Matching time	1 hour 53 minutes
Matching memory usage	3.88 GB
Alignment time	51 minutes 16 seconds
Alignment memory usage	1.19 GB
Optimisation parameters	
Parameters	F, b1, b2, cx, cy, k1-k4, p1, p2
Adaptive camera model fitting	No
Optimization time	8 minutes 39 seconds
Software version	1.6.2.10247
Depth Maps	
Count	1291
Depth maps generation parameters	
Quality	Medium
Filtering mode	Mild
Processing time	10 hours 54 minutes
Software version	1.6.2.10247
Dense Point Cloud	
Points	113,315,226
Point colors	3 abnds, uint8
Depth maps generation parameters	

Quality	Medium
Filtering mode	Mild
Processing time	10 hours 54 minutes
Dense cloud generation parameters	
Processing time	1 hour 22 minutes
Software version	1.6.2.10247
Model	
Faces	22,566,845
Vertices	11,292,011
Vertex colours	3 bands uint8
Depth maps generation parameters	
Quality	Medium
Filtering mode	Mild
Processing time	10 hours 54 minutes
Reconstruction Parameters	
Surface type	Height field
Source data	Dense cloud
Interpolation	Enabled
Strict volumetric masks	No
Processing time	13 minutes 15 seconds
Software version	1.6.2.10247
DEM	
Size	18,099 x 14,292
Coordinate system	GDA94 / MGA zone 56 (EPSG::28356)
Reconstruction parameters	
Source data	Mesh
Interpolation	Enabled
Processing time	6 minutes 24 seconds
Software version	1.6.2.10247
Orthomosaic	
Size	55,560 x 43,688
Coordinate system	GDA94 / MGA zone 56 (EPSG::28356)
Colours	3 bands, uint8
Reconstruction parameters	
Blending mode	Mosaic
Surface	DEM
Enable hole filling	Yes
Processing time	45 minutes 16 seconds
Software Version	1.6.2.10247
System	
Software name	Agisoft Metashape Professional
Software version	1.6.2 build 10247
OS	Windows 64 bit
RAM	31.96 GB
CPU	Intel(R) Xeon(R) CPU E31270 @ 3.40GHz
GPU(s)	None

9.2 Grainsize Classes

Sediment grainsize classes (μm) from Malvern Mastersizer 2000 laser particle size analyser. Eg. The first class is 0.01 μm – 0.0011482 μm.

0.01	0.011482	0.013183	0.015136	0.017378	0.019953	0.022909
0.026303	0.0302	0.034674	0.039811	0.045709	0.052481	0.060256
0.069183	0.079433	0.091201	0.104713	0.120226	0.138038	0.158489
0.18197	0.20893	0.239883	0.275423	0.316228	0.363078	0.416869
0.47863	0.549541	0.630957	0.724436	0.831764	0.954993	1.096478
1.258925	1.44544	1.659587	1.905461	2.187762	2.511886	2.884031
3.311311	3.801894	4.365158	5.011872	5.754399	6.606934	7.585776
8.709636	10	11.48154	13.18257	15.13561	17.37801	19.95262
22.90868	26.30268	30.19952	34.67369	39.81072	45.70882	52.48075
60.25596	69.1831	79.43282	91.20108	104.7129	120.2264	138.0384
158.4893	181.9701	208.9296	239.8833	275.4229	316.2278	363.0781
416.8694	478.6301	549.5409	630.9573	724.436	831.7638	954.9926
1096.478	1258.925	1445.44	1659.587	1905.461	2187.762	2511.886
2884.032	3311.311	3801.894	4365.158	5011.872	5754.399	6606.934
7585.776	8709.636	10000				

Series from Lund University

Department of Physical Geography and Ecosystem Science

Master Thesis in Geographical Information Science

1. *Anthony Lawther:* The application of GIS-based binary logistic regression for slope failure susceptibility mapping in the Western Grampian Mountains, Scotland (2008).
2. *Rickard Hansen:* Daily mobility in Grenoble Metropolitan Region, France. Applied GIS methods in time geographical research (2008).
3. *Emil Bayramov:* Environmental monitoring of bio-restoration activities using GIS and Remote Sensing (2009).
4. *Rafael Villarreal Pacheco:* Applications of Geographic Information Systems as an analytical and visualization tool for mass real estate valuation: a case study of Fontibon District, Bogota, Columbia (2009).
5. *Siri Oestreich Waage:* a case study of route solving for oversized transport: The use of GIS functionalities in transport of transformers, as part of maintaining a reliable power infrastructure (2010).
6. *Edgar Pimiento:* Shallow landslide susceptibility – Modelling and validation (2010).
7. *Martina Schäfer:* Near real-time mapping of floodwater mosquito breeding sites using aerial photographs (2010).
8. *August Pieter van Waarden-Nagel:* Land use evaluation to assess the outcome of the programme of rehabilitation measures for the river Rhine in the Netherlands (2010).
9. *Samira Muhammad:* Development and implementation of air quality data mart for Ontario, Canada: A case study of air quality in Ontario using OLAP tool. (2010).
10. *Fredros Oketch Okumu*: Using remotely sensed data to explore spatial and temporal relationships between photosynthetic productivity of vegetation and malaria transmission intensities in selected parts of Africa (2011).
11. *Svajunas Plunge:* Advanced decision support methods for solving diffuse water pollution problems (2011).
12. *Jonathan Higgins:* Monitoring urban growth in greater Lagos: A case study using GIS to monitor the urban growth of Lagos 1990 - 2008 and produce future growth prospects for the city (2011).
13. *Mårten Karlberg:* Mobile Map Client API: Design and Implementation for Android (2011).
14. *Jeanette McBride:* Mapping Chicago area urban tree canopy using color infrared imagery (2011).
15. *Andrew Farina:* Exploring the relationship between land surface temperature and vegetation abundance for urban heat island mitigation in Seville, Spain (2011).
16. *David Kanyari*: Nairobi City Journey Planner: An online and a Mobile Application (2011).
17. *Laura V. Drews:* Multi-criteria GIS analysis for siting of small wind power plants - A case study from Berlin (2012).
18. *Qaisar Nadeem:* Best living neighborhood in the city - A GIS based multi criteria evaluation of ArRiyadh City (2012).
19. *Ahmed Mohamed El Saeid Mustafa:* Development of a photo voltaic building rooftop integration analysis tool for GIS for Dokki District, Cairo, Egypt (2012).

20. *Daniel Patrick Taylor*: Eastern Oyster Aquaculture: Estuarine Remediation via Site Suitability and Spatially Explicit Carrying Capacity Modeling in Virginia's Chesapeake Bay (2013).
21. *Angeleta Oveta Wilson:* A Participatory GIS approach to *unearthing* Manchester's Cultural Heritage '*gold mine'* (2013).
22. *Ola Svensson:* Visibility and Tholos Tombs in the Messenian Landscape: A Comparative Case Study of the Pylian Hinterlands and the Soulima Valley (2013).
23. *Monika Ogden:* Land use impact on water quality in two river systems in South Africa (2013).
24. *Stefan Rova:* A GIS based approach assessing phosphorus load impact on Lake Flaten in Salem, Sweden (2013).
25. *Yann Buhot:* Analysis of the history of landscape changes over a period of 200 years. How can we predict past landscape pattern scenario and the impact on habitat diversity? (2013).
26. *Christina Fotiou:* Evaluating habitat suitability and spectral heterogeneity models to predict weed species presence (2014).
27. *Inese Linuza:* Accuracy Assessment in Glacier Change Analysis (2014).
28. *Agnieszka Griffin:* Domestic energy consumption and social living standards: a GIS analysis within the Greater London Authority area (2014).
29. *Brynja Guðmundsdóttir:* Detection of potential arable land with remote sensing and GIS - A Case Study for Kjósarhreppur (2014).
30. *Oleksandr Nekrasov:* Processing of MODIS Vegetation Indices for analysis of agricultural droughts in the southern Ukraine between the years 2000-2012 (2014).
31. *Sarah Tressel:* Recommendations for a polar Earth science portal in the context of Arctic Spatial Data Infrastructure (2014).
32. *Caroline Gevaert:* Combining Hyperspectral UAV and Multispectral Formosat-2 Imagery for Precision Agriculture Applications (2014).
33. *Salem Jamal-Uddeen:* Using GeoTools to implement the multi-criteria evaluation analysis - weighted linear combination model (2014).
34. *Samanah Seyedi-Shandiz:* Schematic representation of geographical railway network at the Swedish Transport Administration (2014).
35. *Kazi Masel Ullah:* Urban Land-use planning using Geographical Information System and analytical hierarchy process: case study Dhaka City (2014).
36. *Alexia Chang-Wailing Spitteler:* Development of a web application based on MCDA and GIS for the decision support of river and floodplain rehabilitation projects (2014).
37. *Alessandro De Martino:* Geographic accessibility analysis and evaluation of potential changes to the public transportation system in the City of Milan (2014).
38. *Alireza Mollasalehi:* GIS Based Modelling for Fuel Reduction Using Controlled Burn in Australia. Case Study: Logan City, QLD (2015).
39. *Negin A. Sanati:* Chronic Kidney Disease Mortality in Costa Rica; Geographical Distribution, Spatial Analysis and Non-traditional Risk Factors (2015).
40. *Karen McIntyre:* Benthic mapping of the Bluefields Bay fish sanctuary, Jamaica (2015).
41. *Kees van Duijvendijk:* Feasibility of a low-cost weather sensor network for agricultural purposes: A preliminary assessment (2015).
42. *Sebastian Andersson Hylander:* Evaluation of cultural ecosystem services using GIS (2015).

43. *Deborah Bowyer:* Measuring Urban Growth, Urban Form and Accessibility as Indicators of Urban Sprawl in Hamilton, New Zealand (2015).
44. *Stefan Arvidsson:* Relationship between tree species composition and phenology extracted from satellite data in Swedish forests (2015).
45. *Damián Giménez Cruz*: GIS-based optimal localisation of beekeeping in rural Kenya (2016).
46. *Alejandra Narváez Vallejo:* Can the introduction of the topographic indices in LPJ-GUESS improve the spatial representation of environmental variables? (2016).
47. *Anna Lundgren:* Development of a method for mapping the highest coastline in Sweden using breaklines extracted from high resolution digital elevation models (2016).
48. *Oluwatomi Esther Adejoro:* Does location also matter? A spatial analysis of social achievements of young South Australians (2016).
49. *Hristo Dobrev Tomov:* Automated temporal NDVI analysis over the Middle East for the period 1982 - 2010 (2016).
50. *Vincent Muller:* Impact of Security Context on Mobile Clinic Activities
    A GIS Multi Criteria Evaluation based on an MSF Humanitarian Mission in Cameroon (2016).
51. *Gezahagn Negash Seboka:* Spatial Assessment of NDVI as an Indicator of Desertification in Ethiopia using Remote Sensing and GIS (2016).
52. *Holly Buhler:* Evaluation of Interfacility Medical Transport Journey Times in Southeastern British Columbia. (2016).
53. *Lars Ole Grottenberg*: Assessing the ability to share spatial data between emergency management organisations in the High North (2016).
54. *Sean Grant:* The Right Tree in the Right Place: Using GIS to Maximize the Net Benefits from Urban Forests (2016).
55. *Irshad Jamal:* Multi-Criteria GIS Analysis for School Site Selection in Gorno-Badakhshan Autonomous Oblast, Tajikistan (2016).
56. *Fulgencio Sanmartín:* Wisdom-volkano: A novel tool based on open GIS and time-series visualization to analyse and share volcanic data (2016).
57. *Nezha Acil:* Remote sensing-based monitoring of snow cover dynamics and its influence on vegetation growth in the Middle Atlas Mountains (2016).
58. *Julia Hjalmarsson:* A Weighty Issue: Estimation of Fire Size with Geographically Weighted Logistic Regression (2016).
59. *Mathewos Tamiru Amato:* Using multi-criteria evaluation and GIS for chronic food and nutrition insecurity indicators analysis in Ethiopia (2016).
60. *Karim Alaa El Din Mohamed Soliman El Attar:* Bicycling Suitability in Downtown, Cairo, Egypt (2016).
61. *Gilbert Akol Echelai:* Asset Management: Integrating GIS as a Decision Support Tool in Meter Management in National Water and Sewerage Corporation (2016).
62. *Terje Slinning:* Analytic comparison of multibeam echo soundings (2016).
63. *Gréta Hlín Sveinsdóttir:* GIS-based MCDA for decision support: A framework for wind farm siting in Iceland (2017).
64. *Jonas Sjögren:* Consequences of a flood in Kristianstad, Sweden: A GIS-based analysis of impacts on important societal functions (2017).
65. *Nadine Raska:* 3D geologic subsurface modelling within the Mackenzie Plain, Northwest Territories, Canada (2017).

66. *Panagiotis Symeonidis*: Study of spatial and temporal variation of atmospheric optical parameters and their relation with PM 2.5 concentration over Europe using GIS technologies (2017).
67. *Michaela Bobeck:* A GIS-based Multi-Criteria Decision Analysis of Wind Farm Site Suitability in New South Wales, Australia, from a Sustainable Development Perspective (2017).
68. *Raghdaa Eissa*: Developing a GIS Model for the Assessment of Outdoor Recreational Facilities in New Cities Case Study: Tenth of Ramadan City, Egypt (2017).
69. *Zahra Khais Shahid*: Biofuel plantations and isoprene emissions in Svea and Götaland (2017).
70. *Mirza Amir Liaquat Baig*: Using geographical information systems in epidemiology: Mapping and analyzing occurrence of diarrhea in urban - residential area of Islamabad, Pakistan (2017).
71. *Joakim Jörwall*: Quantitative model of Present and Future well-being in the EU-28: A spatial Multi-Criteria Evaluation of socioeconomic and climatic comfort factors (2017).
72. *Elin Haettner*: Energy Poverty in the Dublin Region: Modelling Geographies of Risk (2017).
73. *Harry Eriksson*: Geochemistry of stream plants and its statistical relations to soil- and bedrock geology, slope directions and till geochemistry. A GIS-analysis of small catchments in northern Sweden (2017).
74. *Daniel Gardevärn:* PPGIS and Public meetings – An evaluation of public participation methods for urban planning (2017).
75. *Kim Friberg:* Sensitivity Analysis and Calibration of Multi Energy Balance Land Surface Model Parameters (2017).
76. *Viktor Svanerud:* Taking the bus to the park? A study of accessibility to green areas in Gothenburg through different modes of transport (2017).
77. *Lisa-Gaye Greene*: Deadly Designs: The Impact of Road Design on Road Crash Patterns along Jamaica's North Coast Highway (2017).
78. *Katarina Jemec Parker*: Spatial and temporal analysis of fecal indicator bacteria concentrations in beach water in San Diego, California (2017).
79. *Angela Kabiru*: An Exploratory Study of Middle Stone Age and Later Stone Age Site Locations in Kenya's Central Rift Valley Using Landscape Analysis: A GIS Approach (2017).
80. *Kristean Björkmann*: Subjective Well-Being and Environment: A GIS-Based Analysis (2018).
81. *Williams Erhunmonmen Ojo*: Measuring spatial accessibility to healthcare for people living with HIV-AIDS in southern Nigeria (2018).
82. *Daniel Assefa*: Developing Data Extraction and Dynamic Data Visualization (Styling) Modules for Web GIS Risk Assessment System (WGRAS). (2018).
83. *Adela Nistora*: Inundation scenarios in a changing climate: assessing potential impacts of sea-level rise on the coast of South-East England (2018).
84. *Marc Seliger*: Thirsty landscapes - Investigating growing irrigation water consumption and potential conservation measures within Utah's largest master-planned community: Daybreak (2018).
85. *Luka Jovičić*: Spatial Data Harmonisation in Regional Context in Accordance with INSPIRE Implementing Rules (2018).

86. *Christina Kourdounouli*: Analysis of Urban Ecosystem Condition Indicators for the Large Urban Zones and City Cores in EU (2018).
87. *Jeremy Azzopardi*: Effect of distance measures and feature representations on distance-based accessibility measures (2018).
88. *Patrick Kabatha*: An open source web GIS tool for analysis and visualization of elephant GPS telemetry data, alongside environmental and anthropogenic variables (2018).
89. *Richard Alphonce Giliba*: Effects of Climate Change on Potential Geographical Distribution of Prunus africana (African cherry) in the Eastern Arc Mountain Forests of Tanzania (2018).
90. *Eiður Kristinn Eiðsson*: Transformation and linking of authoritative multi-scale geodata for the Semantic Web: A case study of Swedish national building data sets (2018).
91. *Niamh Harty*: HOP!: a PGIS and citizen science approach to monitoring the condition of upland paths (2018).
92. *José Estuardo Jara Alvear*: Solar photovoltaic potential to complement hydropower in Ecuador: A GIS-based framework of analysis (2018).
93. *Brendan O'Neill*: Multicriteria Site Suitability for Algal Biofuel Production Facilities (2018).
94. *Roman Spataru*: Spatial-temporal GIS analysis in public health – a case study of polio disease (2018).
95. *Alicja Miodońska*: Assessing evolution of ice caps in Suðurland, Iceland, in years 1986 - 2014, using multispectral satellite imagery (2019).
96. *Dennis Lindell Schettini*: A Spatial Analysis of Homicide Crime's Distribution and Association with Deprivation in Stockholm Between 2010-2017 (2019).
97. *Damiano Vesentini*: The Po Delta Biosphere Reserve: Management challenges and priorities deriving from anthropogenic pressure and sea level rise (2019).
98. *Emilie Arnesten*: Impacts of future sea level rise and high water on roads, railways and environmental objects: a GIS analysis of the potential effects of increasing sea levels and highest projected high water in Scania, Sweden (2019).
99. *Syed Muhammad Amir Raza*: Comparison of geospatial support in RDF stores: Evaluation for ICOS Carbon Portal metadata (2019).
100. *Hemin Tofiq*: Investigating the accuracy of Digital Elevation Models from UAV images in areas with low contrast: A sandy beach as a case study (2019).
101. *Evangelos Vafeiadis*: Exploring the distribution of accessibility by public transport using spatial analysis. A case study for retail concentrations and public hospitals in Athens (2019).
102. *Milan Sekulic*: Multi-Criteria GIS modelling for optimal alignment of roadway by-passes in the Tlokweng Planning Area, Botswana (2019).
103. *Ingrid Piirisaar*: A multi-criteria GIS analysis for siting of utility-scale photovoltaic solar plants in county Kilkenny, Ireland (2019).
104. *Nigel Fox*: Plant phenology and climate change: possible effect on the onset of various wild plant species' first flowering day in the UK (2019).
105. *Gunnar Hesch*: Linking conflict events and cropland development in Afghanistan, 2001 to 2011, using MODIS land cover data and Uppsala Conflict Data Programme (2019).
106. *Elijah Njoku*: Analysis of spatial-temporal pattern of Land Surface Temperature (LST) due to NDVI and elevation in Ilorin, Nigeria (2019).

107. *Katalin Bunyevácz*: Development of a GIS methodology to evaluate informal urban green areas for inclusion in a community governance program (2019).
108. *Paul dos Santos*: Automating synthetic trip data generation for an agent-based simulation of urban mobility (2019).
109. *Robert O' Dwyer*: Land cover changes in Southern Sweden from the mid-Holocene to present day: Insights for ecosystem service assessments (2019).
110. *Daniel Klingmyr*: Global scale patterns and trends in tropospheric NO2 concentrations (2019).
111. *Marwa Farouk Elkabbany*: Sea Level Rise Vulnerability Assessment for Abu Dhabi, United Arab Emirates (2019).
112. *Jip Jan van Zoonen*: Aspects of Error Quantification and Evaluation in Digital Elevation Models for Glacier Surfaces (2020).
113. *Georgios Efthymiou*: The use of bicycles in a mid-sized city – benefits and obstacles identified using a questionnaire and GIS (2020).
114. *Haruna Olayiwola Jimoh*: Assessment of Urban Sprawl in MOWE/IBAFO Axis of Ogun State using GIS Capabilities (2020).
115. *Nikolaos Barmpas Zachariadis*: Development of an iOS, Augmented Reality for disaster management (2020).
116. *Ida Storm*: ICOS Atmospheric Stations: Spatial Characterization of CO2 Footprint Areas and Evaluating the Uncertainties of Modelled CO2 Concentrations (2020).
117. *Alon Zuta*: Evaluation of water stress mapping methods in vineyards using airborne thermal imaging (2020).
118. *Marcus Eriksson*: Evaluating structural landscape development in the municipality Upplands-Bro, using landscape metrics indices (2020).
119. *Ane Rahbek Vierø*: Connectivity for Cyclists? A Network Analysis of Copenhagen's Bike Lanes (2020).
120. *Cecilia Baggini*: Changes in habitat suitability for three declining Anatidae species in saltmarshes on the Mersey estuary, North-West England (2020).
121. *Bakrad Balabanian*: Transportation and Its Effect on Student Performance (2020).
122. *Ali Al Farid*: Knowledge and Data Driven Approaches for Hydrocarbon Microseepage Characterizations: An Application of Satellite Remote Sensing (2020).
123. *Bartlomiej Kolodziejczyk*: Distribution Modelling of Gene Drive-Modified Mosquitoes and Their Effects on Wild Populations (2020).
124. *Alexis Cazorla*: Decreasing organic nitrogen concentrations in European water bodies - links to organic carbon trends and land cover (2020).
125. *Kharid Mwakoba*: Remote sensing analysis of land cover/use conditions of community-based wildlife conservation areas in Tanzania (2021).
126. *Chinatsu Endo*: Remote Sensing Based Pre-Season Yellow Rust Early Warning in Oromia, Ethiopia (2021).
127. *Berit Mohr*: Using remote sensing and land abandonment as a proxy for long-term human out-migration. A Case Study: Al-Hassakeh Governorate, Syria (2021).
128. *Kanchana Nirmali Bandaranayake*: Considering future precipitation in delineation locations for water storage systems - Case study Sri Lanka (2021).
129. *Emma Bylund*: Dynamics of net primary production and food availability in the aftermath of the 2004 and 2007 desert locust outbreaks in Niger and Yemen (2021).

130. *Shawn Pace*: Urban infrastructure inundation risk from permanent sea-level rise scenarios in London (UK), Bangkok (Thailand) and Mumbai (India): A comparative analysis (2021).
131. *Oskar Evert Johansson*: The hydrodynamic impacts of Estuarine Oyster reefs, and the application of drone technology to this study (2021).